NATIONAL TECHNICAL UNIVERSITY OF ATHENS
School of Civil Engineering
Department of Structural Engineering
Institute of Structural Analysis and Antiseismic Research

CONTRIBUTION TO VIBRATION ISOLATION OF WIND TURBINE TOWERS

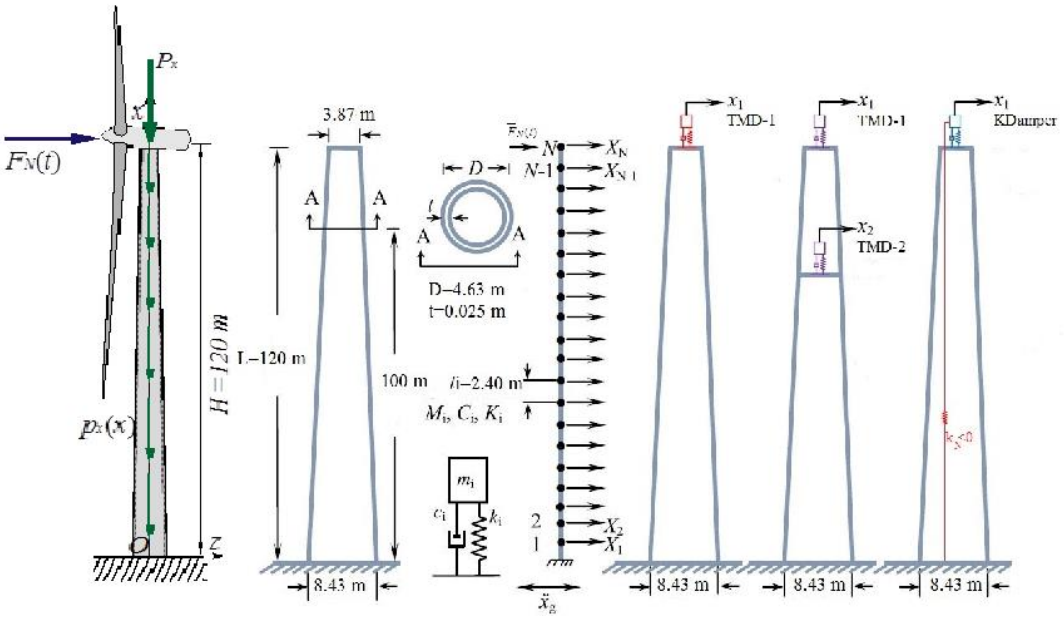

POSTGRADUATE THESIS

Kapasakalis A. Konstantinos

Supervisor: Sapountzakis Evangelos, Professor N.T.U.A.

Athens, July 2017

ΕΘΝΙΚΟ ΜΕΤΣΟΒΙΟ ΠΟΛΥΤΕΧΝΕΙΟ
Σχολή Πολιτικών Μηχανικών
Τομέας Δομοστατικής
Εργαστήριο Στατικής και Αντισεισμικών Ερευνών

ΣΥΜΒΟΛΗ ΣΤΗ ΜΟΝΩΣΗ ΤΑΛΑΝΤΩΣΕΩΝ ΣΕ ΑΝΕΜΟΓΕΝΝΗΤΡΙΕΣ

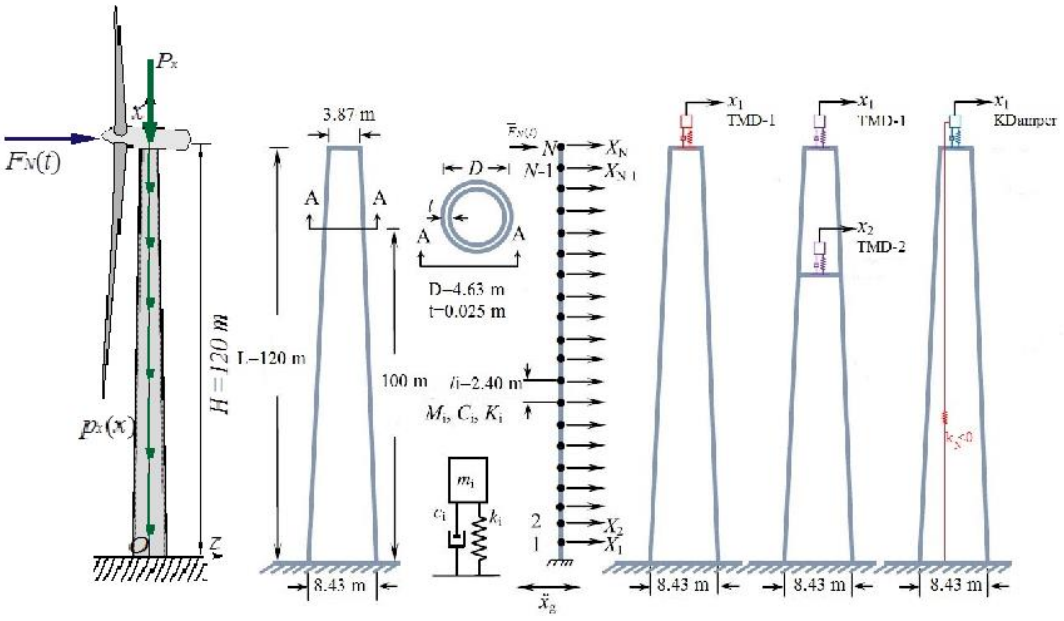

ΜΕΤΑΠΤΥΧΙΑΚΗ ΕΡΓΑΣΙΑ

Καπασακάλης Α. Κωνσταντίνος

Επιβλέπων: Σαπουντζάκης Ευάγγελος, Καθηγητής ΕΜΠ

Αθήνα, Ιούλιος 2017

Kapasakalis A. Konstantinos (2017)

Contribution to vibration isolation of wind turbine towers

Postgraduate Thesis

Institute of Structural Analysis and Antiseismic Research, National Technical University of Athens, Greece

Καπασακάλης Α. Κωνσταντίνος (2017)

Συμβολή στη μόνωση ταλαντώσεων σε ανεμογεννήτριες

Μεταπτυχιακή Εργασία

Εργαστήριο Στατικής και Αντισεισμικών Ερευνών, Εθνικό Μετσόβιο Πολυτεχνείο, Αθήνα.

Στους δικούς μου ανθρώπους,

Θα ήθελα να εκφράσω τις θερμές μου ευχαριστίες στον επιβλέποντα καθηγητή κ. Ε. Σαπουντζάκη για την επιστημονική καθοδήγηση και τη συνεχή βοήθεια που μου προσέφερε κατά την εκπόνηση της εργασίας αυτής.

Επίσης, οφείλω να ευχαριστήσω τους καθηγητές κ. Ι. Αντωνιάδη και κ. Γ. Τσιάτα για την πολύτιμη βοήθειά τους.

Κωστής Καπασακάλης
Ιούλιος 2017

ΕΘΝΙΚΟ ΜΕΤΣΟΒΙΟ ΠΟΛΥΤΕΧΝΕΙΟ
ΣΧΟΛΗ ΠΟΛΙΤΙΚΩΝ ΜΗΧΑΝΙΚΩΝ
ΤΟΜΕΑΣ ΔΟΜΟΣΤΑΤΙΚΗΣ
ΕΡΓΑΣΤΗΡΙΟ ΣΤΑΤΙΚΗΣ ΚΑΙ ΑΝΤΙΣΕΙΣΜΙΚΩΝ ΕΡΕΥΝΩΝ

ΜΕΤΑΠΤΥΧΙΑΚΗ ΕΡΓΑΣΙΑ

Συμβολή στη μόνωση ταλαντώσεων σε ανεμογεννήτριες

Καπασακάλης Α. Κωνσταντίνος

Επιβλέπων: Σαπουντζάκης Ευάγγελος, Καθηγητής ΕΜΠ

ΠΕΡΙΛΗΨΗ

Αντικείμενο της παρούσας εργασίας είναι η μελέτη της δυναμικής συμπεριφοράς των ανεμογεννητριών υπό σεισμικά φορτία και φορτία ανέμου. Πιο συγκεκριμένα, ο πιο κρίσιμος παράγοντας της λειτουργίας των ανεμογεννητριών είναι η κόπωση τόσο του πυλώνα της ανεμογεννήτριας όσο και της θεμελίωσής της. Η κόπωση σχετίζετε ευθέως με τις τάσεις που αναπτύσσονται, οι οποίες με την σειρά τους εξαρτώνται από την δυναμική απόκριση της κατασκευής. Στόχος της εργασίας αυτής είναι η διερεύνηση της επιρροής των συστημάτων μόνωσης, στην μείωση της απόκρισης της κατασκευής, υπό δυναμικά φορτία. Τα συστήματα μόνωσης ταλαντώσεων που εξετάστηκαν είναι το κλασσικό Tuned Mass Damper, σε διάφορες μορφές και διατάξεις, και το καινοτόμο σύστημα μόνωσης KDamper το οποίο συνίσταται στην παθητική μόνωση της κατασκευής ενσωματώνοντας στοιχεία αρνητικής στιβαρότητας. Σαν εισαγωγή, παρουσιάζεται στο 1ο κεφάλαιο μια σύντομη αναφορά στα είδη των ανεμογεννητριών και στην επιρροή που έχουν στον σύγχρονο κόσμο. Στο 2ο κεφάλαιο της εργασίας, αρχικά γίνετε μια βιβλιογραφική αναφορά στα συστήματα μόνωσης Tuned Mass Damper και KDamper. Στη συνέχεια, γίνετε μια σύντομη περιγραφή των συστημάτων αυτών και της λειτουργία τους και μορφώνονται οι εξισώσεις που διέπουν το πρόβλημα ενός μονοβάθμιου ταλαντωτή στον οποίο έχει ενσωματωθεί το αντίστοιχο σύστημα μόνωσης, μορφώνονται οι χαρακτηριστικές εξισώσεις που αφορούν την απόκριση του βαθμού ελευθερίας του μονοβάθμιου ταλαντωτή και εξάγονται συμπεράσματα μετά από βελτιστοποίηση των παραμέτρων των συστημάτων μόνωσης. Στο 3ο κεφάλαιο παρουσιάζεται ο τρόπος που έγινε η μοντελοποίηση, στο πρόγραμμα MATLAB, τόσο της ανεμογεννήτριας χωρίς σύστημα μόνωσης αλλά και της ανεμογεννήτριας με το κάθε ένα από τα συστήματα μόνωσης που εφαρμόστηκαν. Στο 4ο κεφάλαιο, εξάγονται και συγκρίνονται τα αποτελέσματα των δυναμικών παραμετρικών αναλύσεων της ανεμογεννήτριας για όλες τις δυναμικές φορτίσεις και συστήματα μόνωσης που εξετάστηκαν. Τα μεγέθη που θεωρήθηκαν κρίσιμα στα πλαίσια της εργασίας αυτής είναι η μετατόπιση της κορυφής του πυλώνα, διότι είναι άμεσα σχετιζόμενη με τις αναπτυσσόμενες τάσεις και άρα με την κόπωση που αυτές προκαλλούν και η σχετική μετατόπιση μεταξύ της κορυφής του πυλώνα και του εκάστοτε συστήματος μόνωσης.

NATIONAL TECHNICAL UNIVERSITY OF ATHENS
SCHOOL OF CIVIL ENGINEERING
DEPARTMENT OF STRUCTURAL ENGINEERING
INSTITUTE OF STRUCTURAL ANALYSIS AND ANTISEISMIC RESEARCH

POSTGRADUATE THESIS

Contribution to vibration isolation of wind turbine towers

Kapasakalis A. Konstantinos

Supervisor: Sapountzakis Evangelos, Professor N.T.U.A.

ABSTRACT

The subject of this master thesis is the study of the dynamic behavior of wind turbines under seismic and wind loads. More specifically, the critical factor for the function of wind turbines is fatigue, both for the wind turbine tower and for the foundation. The fatigue is directly related to the stress of the tower, the foundation and the dynamic response of the wind turbine. The purpose of this master thesis is the investigation of the influence that the isolation systems have, in the degradation of the response of the structure, under dymanic loads. The isolation systems that are taken into consideration are the classical Tuned Mass Damper, in various implementations, and a novel passive vibration isolation system the KDamper, which incorporates negative stiffness elements in the classical Tuned Mass Damper isolation system. As an introduction to the subject, a brief review in the types of wind turbines and the influence they have in the modern world is presented in Chapter 1. In the second chapter of the thesis, a bibliographic review on the passive isolation systems of Tuned Mass Damper and KDamper is presented. Subsequently, the outline of these isolation systems is presented and the equations that consider a Single Degree of Freedom system combined with the respective isolation system, are formed, and a comparison between them is made after the optimization of their parameters. In the 3rd Chapter, the modeling of the wind turbine tower is described, in the MATLAB environment, for the case of the uncontrolled wind turbine tower and for every implementation of the respective isolation system that is considered. In Chapter 4, the results of the dynamic parametric analysis of the wind turbine tower are being compared for every dynamic load and isolation system that were tested. The factors that were considered critical for this thesis, are the displacement of the top of the tower, because it is closely related to the manifested forces and the fatigue they result in, and the relative displacement of the top of the tower and the isolation system.

CONTENTS

1 INTRODUCTION

In an era of massive energy consumption, alternative energy sources have already been established within our conscience as the last available link between this planet's sustainability and our own very existence. Among these sources, wind turbines are becoming all the more popular, since, with the progress of technology, such constructions promise to provide more efficient and simultaneously less expensive wind power utilization. Observing the evolution of wind power plants, from the windmills of the ancient times to today's modern wind turbines (see Fig. 1.1), one can easily notice the significant changes which have taken place to both the design characteristics and the overall performance of these plants. As time goes by, several aspects, regarding the aerodynamic elements of the rotor, the electrical mechanisms for power extraction, even the areas at which the wind power plants are installed, have been optimized, as to provide the highest possible power output. However huge the changes, though, power still depends on the very same factors on which it always did.

Figure 1.1: Evolution of wind power plants from the ancient Chinese vertical-axis windmill for pumping water (left) to the modern horizontal-axis wind turbine for electrical power extraction (right).

Figure 1.2: First Wind Turbine (Poul La Cour).

Wind turbines have 2 main categories, the horizontal axis and the vertical axis.

- Vertical-axis wind turbines (VAWTs) are a type of wind turbine where the main rotor shaft is set transverse to the wind (but not necessarily vertically) while the main components are located at the base of the turbine.
- Horizontal-axis wind turbines (HAWTs) have the main rotor shaft and electrical generator at the top of a tower, and must be pointed into the wind. Small turbines are pointed by a simple wind wave, while large turbines generally use a wind sensor coupled with a servo motor. Most have a gearbox, which turns the slow rotation of the blades into a quicker rotation that is more suitable to drive an electrical generator.

(a) (b)

Figure 1.3: (a) Horizontal-axis wind turbine and (b) Vertical-axis wind turbine (Darrieus).

World wind power generation capacity has reached 435 GW at the end of 2015, around 7% of total global power generation capacity. A record of 64 GW was added in 2015. The global growth rate of 17.2% was higher than in 2014 (16.4%).

China has once more underpinned its role as the global wind power leader, adding 33 GW of new capacity. This represents a market share of 51.8%. The US market saw good performance with 8.6 GW of added capacity, the strongest growth since 2012. Germany, in anticipation of changes in legislation, installed 4.9 GW. Brazil was the fourth largest market for new turbines with a market volume of 2.8 GW. India saw 2.3 GW of new installations by November 2015.

Global wind power generation amounted to 950 TWh in 2015, nearly 4% of total global power generation. Some countries have reached much higher percentages. Denmark produced 42% of its electricity from wind turbines in 2015 year, the highest figure yet recorded worldwide. In Germany wind power contributed a new record of 13% of the country's power demand in 2015.

The wind power market can be divided into large wind onshore (422 GW, around 210,000 machines), small wind onshore (less than 1 GW installed end 2015, more than 800,000 machines), and offshore (around 12 GW installed end 2015, around 4,000 machines). Large onshore and offshore wind turbines are typically arranged in a wind park. The largest

wind parks exceed 1 GW in size, such as Gansu Wind Farm in China, Muppandal Wind Park in India or Alta Wind Energy Center in USA.

Table 1.1: Top wind power capacity by country, END-2015. Source: WWEA (2016)

Country	Total Capacity (MW)	Added Capacity in 2015 (MW)
China	148000	32970
United States	74347	8598
Germany	45192	4919
India	24759	2294
Spain	22987	0
United Kingdom	13614	1174

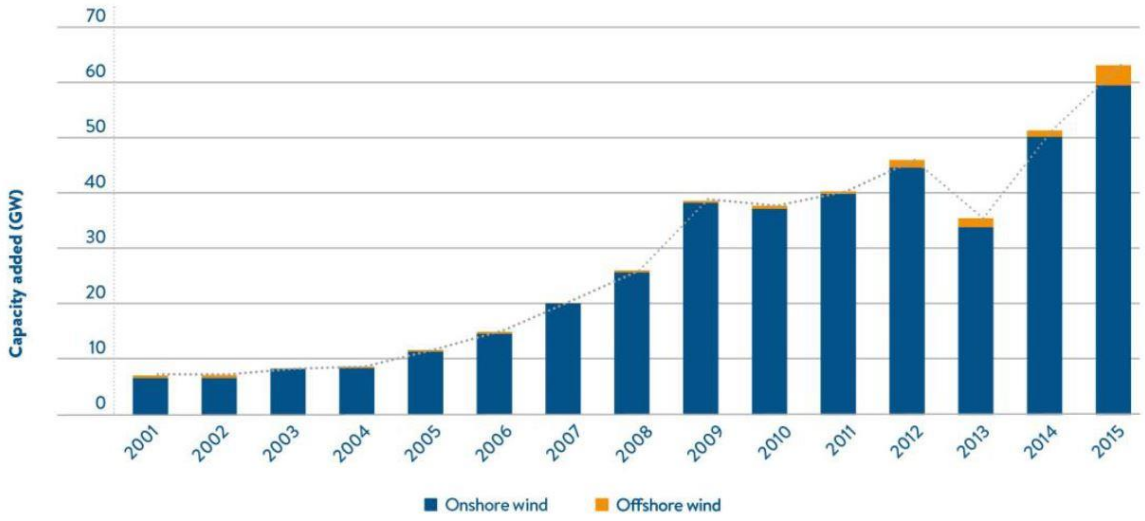

Figure 1.4: Annual net global wind capacity additions, 2001-2015. Source: IRENA, GWEC

Onshore wind is one of the cheapest renewable sources in Australia, Brazil (besides hydro), Germany, Mexico, New Zealand (besides hydro and geothermal), South Africa and Turkey. Global weighted-average installed costs of onshore wind have significantly decreased from US$4,766 per kW in 1983 to US$1,623 per kW in 2014, meaning this a decline in the costs of two-thirds1.

The average cost per kW of onshore wind has declined by 7% and levelised cost of electricity by 12%, for each doubling of installed cumulative over the period 1983 to 2014.2 The global weighted average LCOE of onshore wind could decline by between 20% and 30% by 2025, depending on at least two major factors: technology incremental progress and the cost of capital. Costs are considerably higher for offshore wind because of the additional cost for foundations and connection of the offshore wind parks to the grid. The weighted average cost

per unit of capacity was US$4,650 per kW in 2015, with generation cost in excess of US$15 cents per kWh. However, offshore wind is still in its infancy compared to onshore wind, with total installed capacity having reached 12 GW at the end of 2015. The next generation of advanced large offshore wind turbines, reduced costs for foundations and more efficient project development practices could reduce the LCOE of offshore wind from US$19.6 cents per kWh in 2015 to roughly 12 cents per kWh in 2030.3.

Wind power benefits from government support schemes. The type of support varies by country. Feed in tariffs, feed in renewable portfolio standards in combination with auctions, and production tax credits are among the support schemes that are deployed. Apart from the financial support wind power is usually granted preferential access and additional cost for grid management caused by wind variability are usually not borne by the wind generators. Direct subsidies for new wind generation are falling as the cost of wind power is today on par or below those of fossil and nuclear power generation.

An important issue for managing power systems that integrate large amounts of wind energy is the variability of the power output. The output grows with rising wind speed and it is constant above the rated wind speed. Wind turbines do not produce during periods of low wind speed and they may also stop producing at very high wind speeds. Wind speeds can change significantly on a timescale of minutes. The output of wind turbines is therefore variable. One way to achieve a higher share of wind generation in a grid system is to operate wind turbines or wind farms using integrated transmission systems and power output prediction systems, including weather forecasting. The development of standards and certifications can help to improve the performance of small wind systems, especially in developing countries.

Wind turbines have got progressively bigger, and more powerful. The size of wind turbines has continued to increase, and the average nominal rating of new grid-connected onshore turbines rose from 0.05 megawatts (MW) in 19859 to 2.0 MW in 201410. The largest commercially available turbines to date have a nominal rating of 8.0 MW and, a rotor diameter of 164 meters.

The three major elements of wind generation are the turbine type (vertical/horizontal-axis), installation characteristic (onshore/offshore) and grid connectivity (connected/stand-alone). Most large wind turbines are up-wind horizontal-axis turbines with three blades. Most small wind turbines (SWT) are also horizontal-axis. Innovative designs for vertical-axis turbines are being applied in urban environments, particularly in China. With aerodynamic energy loss of 50-60% at the blade and rotor, mechanical loss of 4% at the gear, and a further 6% electromechanical loss at the generator, overall generation efficiency is typically 30-40%. The majority of today's turbines are designed and built to commercial (i.e. utility) scale; the average turbine rated at 2-3 MW capacity.

There is a wide range of small-scale turbines from 'micro SWTs' rated at less than 1 kW, to 'midi SWTs' reaching 100 kW. SWTs are commonly used as stand-alone electricity systems and frequently applied in isolated locations where the main grid is not accessible. Hybrid wind-diesel systems can improve the stability of power supply in small and off-grid areas, while reducing the costs for fuel and fuel transport by utilizing the existing diesel-based generating infrastructure. However, small wind presents lower load factors and higher capital cost per kW than bigger wind farms, as well as high planning costs per installed unit. Major challenges of small wind include the assessment of the wind resource and the reduction of turbulence's negative effects on the wind resource at the tower's height. High towers reduce the negative impacts of turbulence in the wind resource caused by obstacles in the surroundings, but they increase the costs of small wind turbines. The rapidly declining costs of com-

peting technologies, such as solar, also poses challenges to small wind deployment. Innovation opportunities emerge with these challenges to increase the efficiency and reduce the costs of small wind technology.

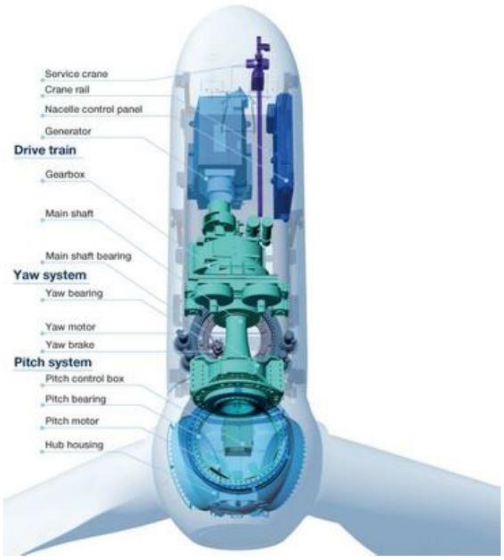

Figure 1.5: Powertrain of a wind turbine. Source: Hitachi

As the power available from the wind increases with the cube its wind speed, all wind turbines need to limit the power output in very high wind speeds. There are two principal means of accomplishing this, with pitch control on the blades or with fixed, stall-controlled blades. Pitch-controlled blades are rotated as wind speeds increase so as to limit the power output and, once the 'rated power' is reached; a reasonably steady output can be achieved, subject to the control system response. Stall-controlled rotors have fixed blades which gradually stall as the wind speed increases, thus limiting the power by passive means. These dispense with the necessity for a pitch control mechanism, but it is rarely possible to achieve constant power as wind speeds rise. Once peak output is reached the power tends to fall off with increasing wind speed, and so the energy capture may be less than that of a pitch-controlled machine. In the early days of the industry, the merits of the two designs were finely balanced and roughly equal numbers of each type were being built. Since the turn of the century, however, pitch-controlled machines have become much more popular. This is due to advances in pitch control, which allow larger and lighter machines compared to stall technology. Another reason is the lower efficiencies attained with stall systems when the wind speed is too high and the rotational speed is therefore decreased.

Initially, conventional wind turbines operated at a fixed (rated) speed when producing power, by starting from a parked position and accelerating due to the wind until it reaches the rated speed. At this point, a connection to the electricity grid is made, and the rotor speed is maintained using either pitch or stall control. Now, variable-speed operation, where the rotor is continuously matched with wind speed, is becoming more common. This means that the rotor can operate at wind speeds below and above rated speed, hence increasing energy capture, and operation at high wind speeds relieves loading on the rotor blades and reduces the

variability of power output. In addition, direct drive turbine systems are becoming increasingly popular, as they eliminate the requirement for a gearbox.

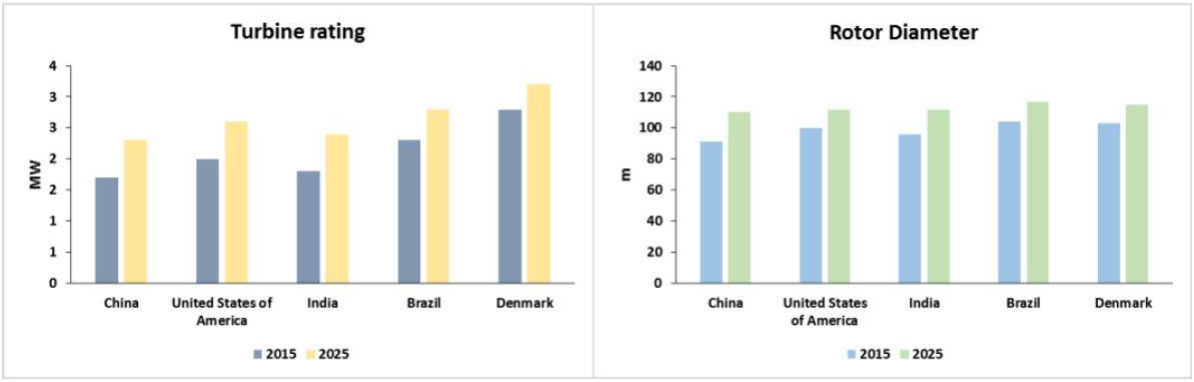

Figure 1.6: Historical and Projected turbine rating and rotor diameter in selected markets. Source: IRENA (forthcoming), MAKE CONSULTING (2015), and the Danish Energy Agency (2016).

2 OVERVIEW OF CONVENTIONAL VIBRATION ABSORBERS AND THE KDAMPER CONCEPT

2.1 GENERAL

The Tuned Mass Damper (TMD) has a long history, already more than 100 years. The TMD concept was first applied by (Frahm, 1909). A theory for the TMD was presented later in the paper by (Ormondroyd and Den Hartog, 1928) . A detailed discussion of optimal tuning and damping parameters appears in (Den Hartog, 1956). Since then, numerous applications of various forms of TMDs have been reported. Some recent examples include vibration absorption in seismic or other forms of excitation of structures (Debnath et al., 2015), wind and wave excitation in wind turbines by (Jun Ling Chen and Georgakis, 2015) and torsional vibrations in rotating and reciprocating machines by (Mayet and Ulbrich, 2015). TMDs are available in various physical forms, including solids, liquids (Jun Ling Chen and Georgakis, 2015), or even active implementations (Younespour and Ghaffarzadeh, 2015). The essential limitation of the TMD is that a large oscillating mass is required in order to achieve significant vibration reduction. Among others, this has prohibited the usage of TMDs in the automotive or aerospace sector.

In an attempt to reduce the requirements for heavy oscillating masses, the inerter concept has been introduced in early 2000s by (Smith, 2002). The inerter is a two terminal element which has the property that the force generated at its ends is proportional to the relative acceleration of its terminals. This constant of proportionality is called “inertance” and is measured in kilograms. The main advantage of the inerter is that the inerter need not have large mass in order to achieve the same inertia effect as the additional mass of the TMD. However, according to (Chen and Smith, 2009) since inerters, dampers and springs can be connected in multiple configurations, the comparison of the structure of the Frequency Response functions of the inerter and of the TMD becomes very complicated. In 2005 the inerter was profitably used as a part of suspension in Formula 1 racing car under the name of “J-damper” (Chen et al., 2009). Since then, other applications emerged, such as in suspensions of railway vehicles (Wang et al., 2012) or in seismic protection of structures (Takewaki et al., 2012). Although the initial inerter configuration is for linear accelerations, rotary versions (Li et al., 2012), or even active configurations (Wand and Wu, 2015) have been proposed. Still, to work efficiently, all considered devices have to be precisely tuned which can be hard to achieve or even impossible in some cases. Moreover, proposed TMDs with inerters suffer

from susceptibility to detuning. Although variable inertance mechanical configurations have been proposed for this purpose (Brzeski et al., 2015), the essential limitation of the inerter is the complex and elaborate mechanical design configurations needed for its implementation.

A parallel direction to the various TMD approaches is the concept of introducing negative stiffness elements (or 'anti-springs') for vibration isolation. This concept has also a long history, being first introduced in the pioneering publication of (Molyneaux, 2015), as well as in the milestone developments of (Platus, 1999). The central concept of these approaches is to significantly reduce the stiffness of the isolator and consequently to reduce the natural frequency of the system even at almost zero levels (Carella et al., 2007), being thus called "Quazi Zero Stiffness" (QZS) oscillators. In this way, the transmissibility of the system for all operating frequencies above the natural frequency is reduced, resulting to enhanced vibration isolation. An initial comprehensive review of such designs can be found in (Ibrahim, 2008).

The negative stiffness behavior is primarily achieved by special mechanical designs involving conventional positive stiffness pre-stressed elastic mechanical elements, such as post-buckled beams, plates, shells and pre-compressed springs, arranged in appropriate geometrical configurations. Some interesting designs are described in (Winterflood et al., 2002),(Virgin et al.,2008). However, alternatively to elastic forces, other forms of physical forces can be used to produce an equivalent negative stiffness effect, such as gravitational (Dyskin and Pasternak, 2012), magnetic (Robertson et al., 2009) or electromagnetic (Zhou and Liu, 2010). Quazi Zero Stiffness (QZS) oscillators are finding numerous applications in seismic isolation (DeSalvo, 2007), (Iemura and Pradono, 2009), (Sarlis et al., 2012), (Attary et al., 2015) in all types of automotive suspensions (Lee et al., 2007), (Le and Ahn, 2011), (Lee and Goverdovskyi, 2012) or in torsional vibrations (Zhou and Xu, 2015). Quite recently, periodic cellular structures with advanced dynamic behavior have been also proposed (Virk et al., 2013), (Bravelli and Ruzzene, 2013), (Michelis and Spitas, 2010), (Correa et al., 2015), combining high positive and negative stiffness. Although the physical mechanisms that generate increased damping in cellular structures are not well understood, micro-buckling or slip- stick phenomena (Lakes et al., 1993), (Spitas et al., 2013), (Chortis et al., 2013) could be among the possible explanations.

Parallel, quite interesting possibilities towards achieving significant damping have been demonstrated to exist also in materials comprising a negative stiffness phase (Lakes, 2001), not only at a material level (Jaglinski, 2007), but also at macroscopic devices (Dong and Lakes, 2013). Moreover, such a behaviour can be combined with high stiffness properties. A theoretical approach has been performed for the analysis of the static and dynamic stability of composite materials, incorporating negative stiffness elements (Wojnar and Kochmann, 2014).

However, Quazi Zero Stiffness (QZS) oscillators suffer from their fundamental requirement for a drastic reduction of the stiffness of the structure almost to negligible levels, which limits the static load capacity of such structures.

For the completeness of the review, it should be mentioned that a rich variety of nonlinear dynamic phenomena (Vakakis et al., 2008), (Farid and Gendelman, 2008), (Lee et al., 2004), (Carella et al., 2012), (Kovacic et al., 2008), (Shaw et al., 2013), either inherently present, or designed to be present in all types of the above vibration absorbers, greatly contribute to the complexity of their dynamic behavior, as well as to the increase of their dynamic performance. However, their treatment is far beyond the scope of this paper. In any case, they can be used to act complimentary to the above vibration absorption concept.

Quite recently, a novel type of oscillator has been proposed (Antoniadis et al., 2015), incorporating a negative stiffness element, which can exhibit extraordinary damping properties, without presenting the drawbacks of the traditional linear oscillator, or of the 'zero-stiffness' designs. This oscillator is designed to present the same overall (static) stiffness as a traditional reference original oscillator. However, it differs both from the original SDoF oscillator, as well as from the known negative stiffness oscillators, by appropriately redistributing the individual stiffness elements and by reallocating the damping. Although the proposed oscillator incorporates a negative stiffness element, it is designed to be both statically and dynamically stable. Once such a system is designed according to the approach proposed in (Antoniadis et al., 2015), it is shown to exhibit an extraordinary damping behaviour. Moreover, a drastic increase of several orders of magnitude has been observed for the damping ratio of the flexural waves propagating within layered periodic structures incorporating such negative stiffness oscillators (Chronopoulos et al., 2015).

In this study, the concept of (Antoniadis et al., 2015) is treated in a systematic way, within the context of the design of a general class of tuned mass dampers. An overview of the dynamic structure of the main conventional vibration absorbers/isolators is presented, -the Quazi Zero Stiffness Oscillator, the Tuned Mass damper and the Inerter- together with a concise presentation of their disadvantages. Next the KDamper is introduced, together with a preliminary conceptual presentation on its fundamental concept and on the reasons why this concept offers the potential to overcome the disadvantages of the traditional vibration absorbers. The optimal selection approach of the KDamper parameters is introduced, which follows exactly the same steps of (Den Hartog, 1956). In this way, a direct comparison of the KDamper with the TMD is performed, which reveals its basic properties. The KDamper always indicates better isolation properties than a TMD damper with the same additional mass. Instead of increasing the additional mass, the vibration isolation capability of the KDamper can be increased by increasing the value of the negative stiffness element. Consequently, significant vibration isolation properties can be achieved, even for very low values (practically insignificant) of the additional mass. However, the increase of the negative stiffness element is upper bounded by the static stability limit of the structure.

Figure 2.1 presents the basic layout of the fundamental vibration isolation and damping concepts to be considered. They are all designed to minimize the response *x(t)* of an un-damped SDoF system of mass *m* and total static stiffness *k* of to an external excitation force *f(t)*.

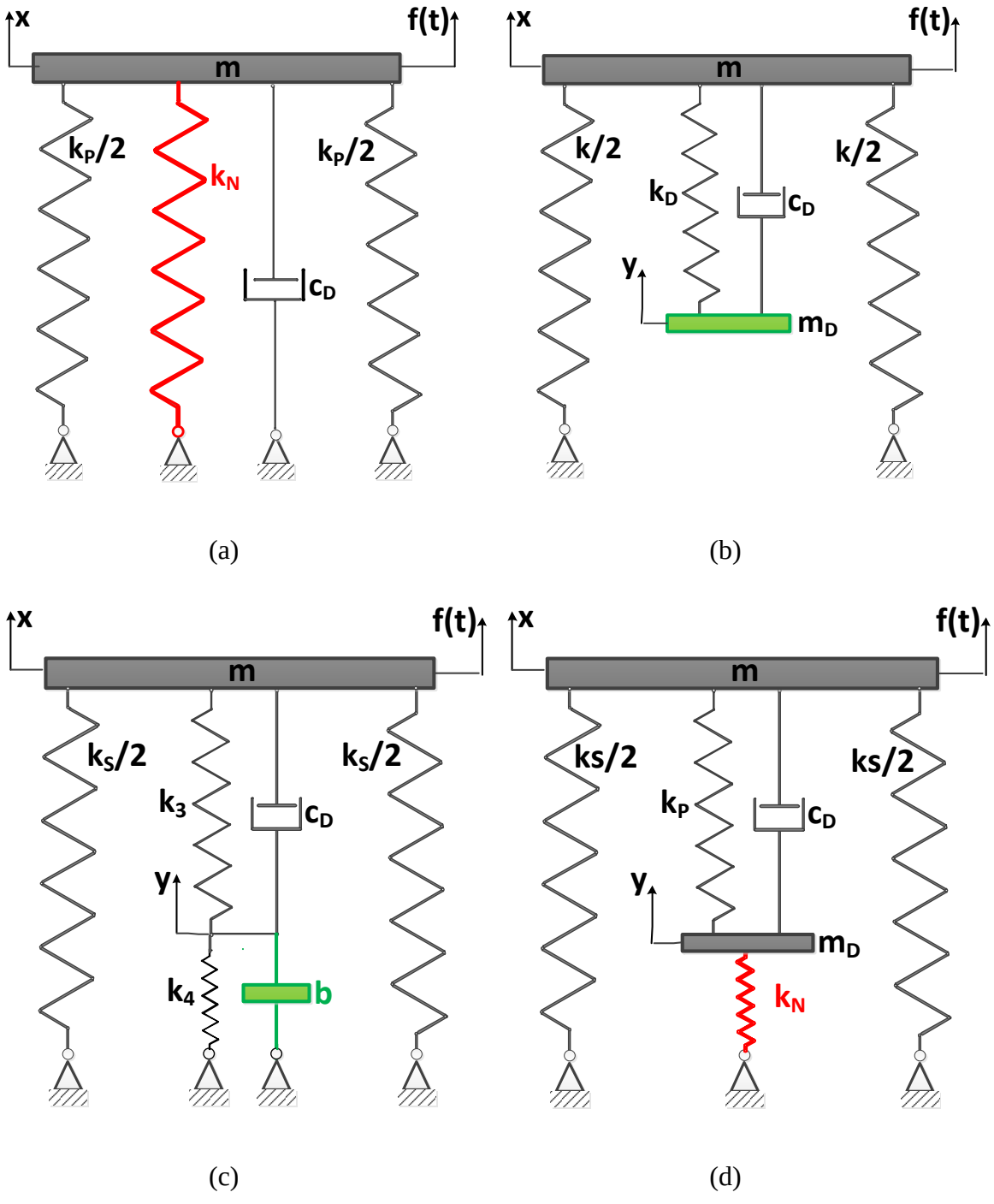

Figure 2.1: Schematic presentation of the considered vibration absorption concepts (a) Quasi-Zero Stiffness (QZS) oscillator, (b) Tuned Mass Damper(TMD), (c) Inerter (JDamper), (d) KDamper.

2.2 QUAZI ZERO STIFFNESS OSCILLATOR

The concept of the QZS oscillator, presented in Fig.2.1a, is to add a negative stiffness element k_N in parallel to the conventional positive stiffness element k_P . The equation of motion of the Quazi Zero Stiffness (QZS) oscillator thus becomes:

$$m\ddot{x} + c_D\dot{x} + (k_P + k_N)x = m\ddot{x} + c_D\dot{x} + kx = f \tag{2.1}$$

Since k_N is negative, the overall static stiffness $k = k_N + k_P$ of the system is reduced. This correspondingly reduces the natural frequency f_0 of the system.

$$f_0 = \frac{1}{2\pi}\sqrt{\frac{k}{m}} \tag{2.2}$$

However, this limits the static loading capacity of the structure, which may result to unsolvable problems, especially for vertical vibration isolation. For example, if X_{VSD} denotes the static deflection of such an isolation system under its own weight in the vertical direction:

$$X_{VSD} = \frac{mg}{k} \tag{2.3}$$

the combination of equations (2.2) and (2.3) leads to:

$$X_{VSD} = \frac{g}{(2\pi f_0)^2} \tag{2.4}$$

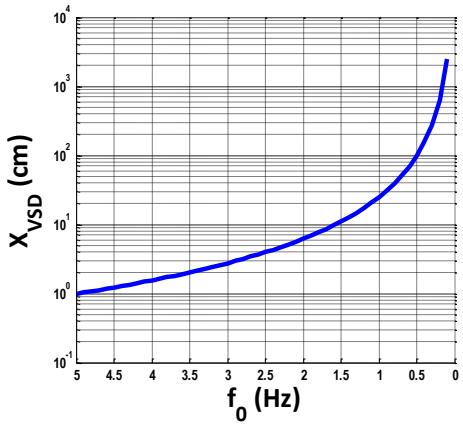

Figure 2.2: Dependence of the static deflection X_{SVD} on the isolation frequency f_0 for vertical vibration isolation.

Fig. 2.2 presents graphically eq. (2.4) and it clearly reflects the implicit constraints for low frequency vibration isolation, especially in the vertical direction. It should be noted that according to eq. (2.4), X_{SVD} depends only on the acceleration of gravity g and on the natural frequency (isolation frequency) f_0.

2.3 CLASSICAL TUNED MASS DAMPER

The concept of the Tuned Mass Damper (TMD) is presented in Fig.2.1b. The resulting equation of motion is:

$$m\ddot{x} + c_D(\dot{x} - \dot{y}) + kx + k_D(x - y) = f \tag{2.5.a}$$

$$m_D\ddot{y} - c_D(\dot{x} - \dot{y}) - k_D(x - y) = 0 \tag{2.5.b}$$

or equivalently:

$$m\ddot{x} + kx + m_D\ddot{y} = f \tag{2.5.c}$$

$$m_D\ddot{y} - c_D(\dot{x} - \dot{y}) - k_D(x - y) = 0 \tag{2.5.d}$$

Assuming a harmonic excitation in the form of:

$$f(t) = kX_{ST} \exp(j\omega t) \tag{2.6}$$

and a steady state response of:

$$x(t) = \tilde{X} \exp(j\omega t) \tag{2.7.a}$$

$$y(t) = \tilde{Y} \exp(j\omega t) \tag{2.7.b}$$

where $\tilde{X}, \tilde{Y}$ denote the complex response amplitudes, the equations of motion (2.5) of the TMD become:

$$-\omega^2 m\tilde{X} + j\omega c_D(\tilde{X} - \tilde{Y}) + k\tilde{X} + k_D(\tilde{X} - \tilde{Y}) = kX_{ST} \tag{2.8.a}$$

$$-\omega^2 m_D\tilde{Y} - j\omega c_D(\tilde{X} - \tilde{Y}) - k_D(\tilde{X} - \tilde{Y}) = 0 \tag{2.8.b}$$

or equivalently:

$$-\omega^2 m\tilde{X} + k\tilde{X} - \omega^2 m_D\tilde{Y} = kX_{ST} \tag{2.8.c}$$

$$-\omega^2 m_D\tilde{Y} - j\omega c_D(\tilde{X} - \tilde{Y}) - k_D(\tilde{X} - \tilde{Y}) = 0 \tag{2.8.d}$$

The resulting transfer function for the response amplitude $\tilde{X}$ is:

$$\tilde{T}_{XM} = \frac{\tilde{X}}{X_{ST}} = \frac{(-\omega^2 m_D + j\omega c_D + k_D)k}{(-\omega^2 m + j\omega c_D + k + k_D)(-\omega^2 m_D + j\omega c_D + k_D) - (j\omega c_D + k_D)^2} \tag{2.9.a}$$

or

$$\tilde{T}_{XM} = \frac{\tilde{X}}{X_{ST}} = \frac{(\rho^2 - q^2) + j2\zeta_D \rho q}{[q^4 - q^2(1+\rho^2+\mu\rho^2) + \rho^2] + j2\zeta_D \rho q[1 - q^2(1+\mu)]} \tag{2.9.b}$$

where:

$$q = \omega / \omega_0 \tag{2.10.a}$$

$$\rho = \omega_D / \omega_0 \tag{2.10.b}$$

$$\omega_0 = \sqrt{k / m} \tag{2.10.c}$$

$$\omega_D = \sqrt{k_D / m_D} \tag{2.10.d}$$

$$\zeta_D = c_D / 2\sqrt{k_D m_D} \tag{2.10.e}$$

$$\mu = m_D / m \tag{2.10.f}$$

An approach for the optimal selection of the TMD parameters ρ and ζ_D (optimal "TMD tuning") can be found among others in (Den Hartog, 1956) and it leads to the following results:

$$\rho_{OPT} = 1/(1+\mu) \tag{2.11.a}$$

$$\zeta_{D_{OPT}} = \sqrt{3\mu / 8(1+\mu)^3} \tag{2.11.b}$$

The maximum value of the amplitude of the transfer function becomes:

$$T_{XM\max} = \frac{X_{MAX}}{X_{ST}} = \frac{\left|\tilde{X}\right|_{MAX}}{X_{ST}} = \sqrt{\frac{2+\mu}{\mu}} = \sqrt{1+2/\mu} \tag{2.12}$$

Figure 2.3 presents the effect of the mass ratio μ on the Transfer function of the TMD. It can be easily noticed that a high value of μ is required for efficient vibration isolation. This fact consists the major disadvantage of the TMD.

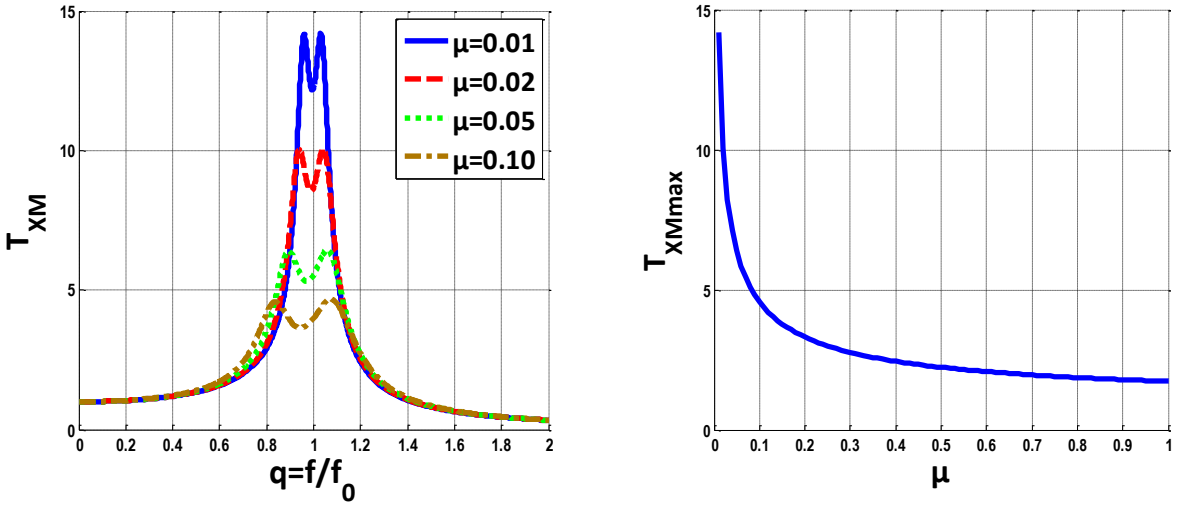

(a) (b)

Figure 2.3: Effect of the mass ratio μ on the Transfer function T_{XM} of the TMD (a)Values of T_{XM} for four different values of μ. (b) Variation of the maximum value T_{XMmax} of the transfer function T_{XM} over μ.

An indicative form of the implementation of the inerter is presented in Fig 1.c. It corresponds to a simplified version of the configuration of case (i) Figure 2.7 of (Chen and Smith, 2009). The equation of motion of this specific configuration of the Inerter is:

$$m\ddot{x} + c_D(\dot{x} - \dot{y}) + k_S x + k_3(x - y) = f \tag{2.13.a}$$

$$b\ddot{y} - c_D(\dot{x} - \dot{y}) - k_3(x - y) + k_4 y = 0 \tag{2.13.b}$$

From a dynamics point of view, the transfer function of the system of equations (2.13) for the inerter is exactly the same as the transfer function of the TMD in Eq (2.8), when the value of k_4 is equal to zero and for $b=m_D$, $k_3=k_D$. Moreover, as it will be further proven , a positive value for k_4 has an adverse effect to the transfer function of the system. Therefore, the main advantage of the inerter over the TMD is considered to be technological: due to the technological design of the inerter, it can achieve the same inertia effect with a TMD, while it requires significantly less added mass than the TMD.

2.4 THE KDAMPER CONCEPT

Figure 2.1.d presents the fundamental concept of the KDamper. Similarly to the QZS oscillator, it uses a negative stiffness element k_N. However, contrary to the QZS oscillator, the first basic requirement of the KDamper is that the overall static stiffness of the system is maintained:

$$k_S + \frac{k_P k_N}{k_P + k_N} = k \tag{2.14}$$

In this way, the KDamper can overcome the fundamental disadvantage of the QZS oscillator. Compared to the TMD damper, and similarly to the inerter, the KDamper also uses a dual port element, which connects the additional mass also to the base. However, instead of an inertial element (i.e. the inerter), the KDamper makes use of a negative stiffness element k_N. Thus, the equation of motion of the KDamper becomes:

$$m\ddot{x} + c_D(\dot{x} - \dot{y}) + k_S x + k_P(x - y) = f \tag{2.15.a}$$

$$m_D\ddot{y} - c_D(\dot{x} - \dot{y}) - k_P(x - y) + k_N y = 0 \tag{2.15.b}$$

or equivalently:

$$m\ddot{x} + k_S x + m_D\ddot{y} + k_N y = f \tag{2.15.c}$$

$$m_D\ddot{y} - c_D(\dot{x} - \dot{y}) - k_P(x - y) + k_N y = 0 \tag{2.15.d}$$

Assuming a harmonic excitation in the form of eq. (2.6) and corresponding harmonic responses in the form of eq. (2.7), the equations of motion (2.15) of the TMD become:

$$-\omega^2 m\tilde{X} + j\omega c_D(\tilde{X} - \tilde{Y}) + k_S\tilde{X} + k_P(\tilde{X} - \tilde{Y}) = kX_{ST} \tag{2.16.a}$$

$$-\omega^2 m_D\tilde{Y} - j\omega c_D(\tilde{X} - \tilde{Y}) - k_P(\tilde{X} - \tilde{Y}) + k_N\tilde{Y} = 0 \tag{2.16.b}$$

or equivalently:

$$-\omega^2 m\tilde{X} + k_S\tilde{X} - \omega^2 m_D\tilde{Y} + k_N\tilde{Y} = kX_{ST} \tag{2.16.c}$$

$$-\omega^2 m_D\tilde{Y} - j\omega c_D(\tilde{X} - \tilde{Y}) - k_P(\tilde{X} - \tilde{Y}) + k_N\tilde{Y} = 0 \tag{2.16.d}$$

A careful examination of eq. (2.16.c) reveals that the amplitude F_{MD} of the inertia force of the additional mass and the amplitude F_N of the negative stiffness force:

$$F_{MD} = -\omega^2 m_D Y \tag{2.17.a}$$

$$F_N = k_N Y \leq 0 \tag{2.17.b}$$

are exactly in phase, due to the negative value of k_N. Thus, similarly to the inerter, the KDamper essentially consists an indirect approach to increase the inertia effect of the additional mass m_D. Without however increasing the mass m_D itself. This is more obvious by a further comparison of eq. (2.8.c) and (2.16.c). Moreover, it should be noticed that the value of F_{MD} depends on the frequency, while the value of F_N is constant in the entire frequency range, a fact which is of importance for low frequency vibration isolation.

2.4.1 OPTIMAL DESIGN APPROACH FOR THE KDAMPER

The optimal design approach for the parameters of the KD damper follows exactly the corresponding steps as in (Den Hartog, 1956). First, the transfer function of the KD damper results from eq. (2.16).

$$\tilde{T}_{XK} = \frac{\tilde{X}}{X_{ST}} = \frac{(-\omega^2 m_D + j\omega c_D + k_D)k}{(-\omega^2 m + j\omega c_D + k_S + k_P)(-\omega^2 m_D + j\omega c_D + k_D) - (j\omega c_D + k_P)^2} \tag{2.18.a}$$

$$\tilde{T}_{YK} = \frac{\tilde{Y}}{\tilde{X}} \tilde{T}_{XK} = \frac{(j\omega c_D + k_P)k}{(-\omega^2 m_D + j\omega c_D + k_D)} \tilde{T}_{XK} \tag{2.18.b}$$

Where:

$$k_D = k_P + k_N \tag{2.19}$$

and k is defined in (2.14). In view of the fact that k_N is negative and k_D is positive, the parameter κ is defined as:

$$\kappa = -k_N / k_D = -k_N /(k_P + k_N) \tag{2.20}$$

Eq. (2.18) becomes:

$$\tilde{T}_{XK} = \frac{\tilde{\tilde{X}}}{X_{ST}} = \frac{A + (j2\zeta_D)B}{C + (j2\zeta_D)D} \tag{2.21.a}$$

$$\tilde{T}_{YXK} = \frac{\tilde{\tilde{Y}}}{\tilde{\tilde{X}}} = \frac{E + (j2\zeta_D)B}{A + (j2\zeta_D)B} \tag{2.21.b}$$

and consequently:

$$T_{XK} = \frac{\left|\tilde{\tilde{X}}\right|}{X_{ST}} = \frac{X}{X_{ST}} = \sqrt{\frac{A^2 + (2\zeta_D)^2 B^2}{C^2 + (2\zeta_D)^2 D^2}} \tag{2.21.c}$$

$$T_{YXK} = \frac{Y}{X} = \sqrt{\frac{E^2 + (2\zeta_D)^2 B^2}{A^2 + (2\zeta_D)^2 B^2}} \tag{2.21d}$$

$$T_{YK} = \frac{Y}{X_{St}} = \frac{Y}{X}\frac{X}{X_{ST}} = \sqrt{\frac{E^2 + (2\zeta_D)^2 B^2}{C^2 + (2\zeta_D)^2 D^2}} \tag{2.21.e}$$

where:

$$A = \rho^2 - q^2 \tag{2.22.a}$$

$$B = \rho q \tag{2.22.b}$$

$$C = q^4 - q^2[1 + \rho^2 + (1+\kappa)^2 \mu\rho^2] + \rho^2 \tag{2.22.c}$$

$$D = \rho q[(1 + \kappa^2 \mu\rho^2) - q^2(1+\mu)] \tag{2.22.d}$$

$$E = (1+\kappa)\rho^2 \tag{2.22.e}$$

It can be easily verified that for κ=0, eq. (2.21.c) and (2.9.b) are the same. In the limit cases of $\zeta_D = 0$ or $\zeta_D \to \infty$ eq. (2.21.c) becomes:

$$T_{XK}(0) = \left|\frac{A}{C}\right| \tag{2.23.a}$$

$$T_{XK}(\infty) = \left|\frac{B}{D}\right| \tag{2.23.b}$$

The optimal design approach followed in (Den Hartog, 1956), which will be also used in the current paper, is based on the identification of a pair of frequencies q_L <1 and q_R>1, where the values $T_{XK}(q_L)$ and $T_{XK}(q_R)$ become independent of of ζ_D. The first step for the optimization procedure, is the requirement that the values of the transfer functions at these points are equal:

$$T_{XK}(q_L) = T_{XK}(q_R) = T_{XKI} \tag{2.24}$$

In order that a solution for such a pair of frequencies solution exists, two alternative conditions must be fulfilled:

Case I:

$$AD = BC \tag{2.25}$$

The algebraic elaboration of eq. (2.25) results to:

$$\mu(q^2 + \kappa\rho^2)^2 = 0 \tag{2.26}$$

As it can be easily verified, no solution of eq. (2.26) exists for a positive q^2, when the values μ,κ and ρ are positive.

Case II:

$$AD = -BC \tag{2.27}$$

Elaboration of eq. (2.27) results to:

$$(2+\mu)q^4 - 2[1+(1+\mu+\kappa\mu+\kappa^2\mu)\rho^2]q^2 + (2+\kappa^2\mu\rho^2)\rho^2 = 0 \tag{2.28}$$

As a result of eq. (2.28) the pair of roots of eq. (2.28) must satisfy:

$$q_L^2 + q_R^2 = \frac{2[1+(1+\mu+\kappa\mu+\kappa^2\mu)\rho^2]}{2+\mu} \tag{2.29}$$

Additionally, both roots q_L and q_R must fulfill eq. (2.23.b), which results to:

$$\frac{1}{(1+\kappa^2\mu\rho^2) - q_L^2(1+\mu)] } = -\frac{1}{(1+\kappa^2\mu\rho^2) - q_R^2(1+\mu)]} \tag{2.30.a}$$

or equivalently:

$$q_L^2 + q_R^2 = \frac{2(1+\kappa^2\mu\rho^2)}{1+\mu} \tag{2.30.b}$$

The combination of eq. (2.28) and (2.30.b) leads to the optimal value of the parameter ρ in terms of the parameters κ and μ:

$$\rho_{OPT} = \sqrt{\frac{1}{(1+\mu+\kappa\mu)(1+\mu) - \kappa^2\mu}} \tag{2.31}$$

As it can be easily verified, eq. (2.31) is reduced to eq. (2.11.a) in case of κ=0. Substitution of (2.31) into eq. (2.28) leads to the values of the pair q_L and q_R:

$$q_L^2 = \frac{(1+\mu+\kappa\mu)}{2+\mu} - \frac{\sqrt{\Delta}}{2(2+\mu)} \tag{2.32.a}$$

$$q_R^2 = \frac{(1+\mu+\kappa\mu)}{2+\mu} + \frac{\sqrt{\Delta}}{2(2+\mu)} \tag{2.32.b}$$

$$\Delta = 4\frac{2(1+\mu)^2(1+\kappa)^2\mu(2+\mu)}{[(1+\mu+\kappa\mu)(1+\mu)-\kappa^2\mu]^2} \tag{2.32.c}$$

Substitution of either (2.32.a) -or equivalently of (2.32.b)- into eq. (2.23.b) into (2.30.a) leads to:

$$T_{XKI} = T_{XKL} = T_{XK}(q_L) = T_{XKR} = T_{XK}(q_R) = \sqrt{\frac{2+\mu}{\mu}}\tau(\kappa,\mu) = T_{XM\max}.\tau(\kappa,\mu) \tag{2.33.a}$$

$$\tau(\kappa,\mu) = \frac{(1+\mu+\kappa\mu)(1+\mu)-\kappa^2\mu}{(1+\mu)^2(1+\kappa)} = \frac{1}{\rho_{OPT}^2}\frac{1}{(1+\mu)^2(1+\kappa)} \tag{2.33.b}$$

As it can be again easily verified, eq. (2.33.a) is reduced to eq. (2.12) in case of κ=0.

Considering the selection of ζ_D, numerous approaches are possible, the detailed treatment of which is beyond the scope of the current paper. A straightforward approach is followed in the current paper, requiring that for a specified frequency q_Z :

$$T_{XK}(q_Z) = \sqrt{\frac{A^2(q_Z)+(2\zeta_D)^2B^2(q_Z)}{C^2(q_Z)+(2\zeta_D)^2D^2(q_Z)}} = T_{XKI} \Leftrightarrow \zeta_D = \frac{1}{2}\sqrt{-\frac{C^2(q_Z)T_{XKI}^2 - A^2(q_Z)}{D^2(q_Z)T_{XKI}^2 - B^2(q_Z)}} \tag{2.34}$$

A frequent choice for q_S is:

$$q_Z = \sqrt{\rho} \tag{2.35}$$

The values of the elements of the KDamper thus finally result as:

$$k_N / k = \kappa_N = -\kappa\mu\rho^2 \tag{2.36.a}$$

$$k_P / k = \kappa_P = (1+\kappa)\mu\rho^2 \tag{2.36.b}$$

$$k_S / k = \kappa_S = 1+\kappa(1+\kappa)\mu\rho^2 \tag{2.36.c}$$

$$m_D = \mu m \tag{2.36.d}$$

$$c_D = 2\zeta_D \sqrt{(k_P + k_N) m_D} \tag{2.36.e}$$

2.4.2 BASIC PROPETRIES OF THE KDAMPER

Subtraction of the nominator from the denominator in eq. (2.33.b) leads to the following relation:

$$(1+\mu)^2(1+\kappa) - (1+\mu+\kappa\mu)(1+\mu) + \kappa^2\mu = \kappa(1+\mu+\kappa\mu) \geq 0 \tag{2.37}$$

Relation (2.37) implies that:

$$1 \geq \tau(\kappa, \mu) \geq 0 \tag{2.38}$$

Thus, the following PROPERTY 1 of the KDamper is a direct consequence of eq. (2.33.a), (38):

PROPERTY 1: *The amplitude of the transfer function T_{XKI} of the KDamper at the points q_L and q_R is less than the maximum amplitude of the transfer function T_{XMmax} of a TMD with equal μ:*

$$T_{XKI} = T_{XKL} = T_{XKR} \leq T_{XM\max} \tag{2.39}$$

The obvious consequence of PROPERTY 1 is that the addition of a negative stiffness spring reduces the magnitude of the transfer function of the TMD. Figure 2.4 presents the Transfer function of the KDamper for two values of κ. An obvious reduction is observed, compared to Fig 2.3.a.

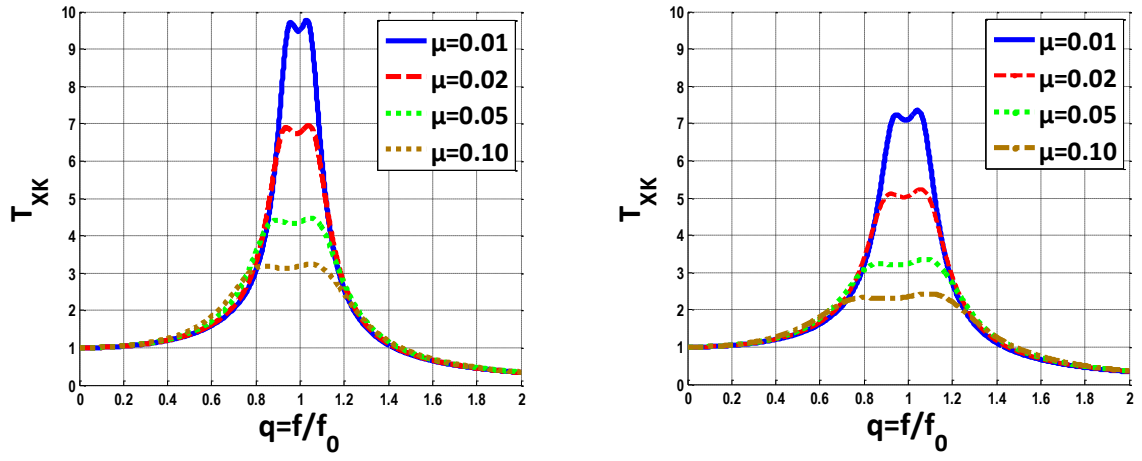

Figure 2.4: Effect of the mass ratio μ on the Transfer function T_{XK} of the KDamper for (a)κ=0.5, (b)κ=1.0.

It should be noted that PROPERTY 1 does not hold for a spring k_N with positive stiffness (i.e. with a negative value of κ). Next, equating the denominator of eq. (2.31) to zero, the following second order equation for κ results:

$$(1+\mu+\kappa\mu)(1+\mu)-\kappa^2\mu=0 \Leftrightarrow \kappa^2\mu-\kappa\mu(1+\mu)-(1+\mu)^2=0 \tag{2.40}$$

Solution of eq. (2.40) leads to the following maximum value that can be reached for κ:

$$\kappa_{MAX}=(1+\mu)\frac{1+\sqrt{1+4/\mu}}{2} \tag{2.41}$$

The first consequence of eq. (2.40) and (2.41) is the following PROPERTY 2.

PROPERTY 2: *The amplitude of the transfer function T_{XKI} of the KDamper at the points q_L and q_R tends to zero when κ reaches the limit value of κ_{MAX}*

$$T_{XKI}=T_{XKL}=T_{XKR}\to 0 \text{ for } \kappa\to\kappa_{MAX} \tag{2.42}$$

The most important consequence of eq. (2.42) is that quite small values of the transfer function T_{XK} can be reached.

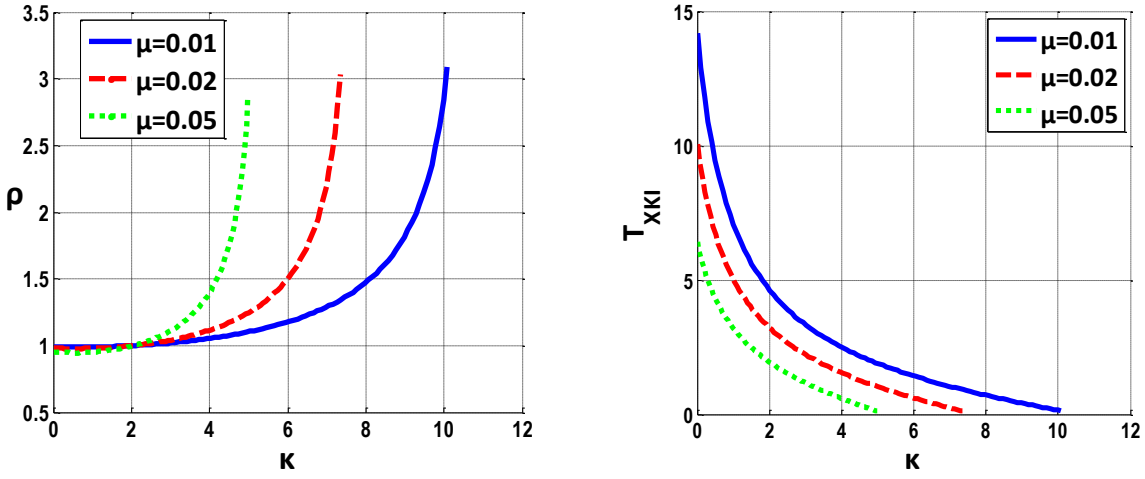

(a) (b)

Figure 2.5: Variation of the KDamper parameters a) Effect of κ and μ the value of $\rho=\omega_D/\omega_0$. B) Effect of κ and μ on the value T_{XKI} of the transfer function T_{XK} at the invariant points q_L, q_R.

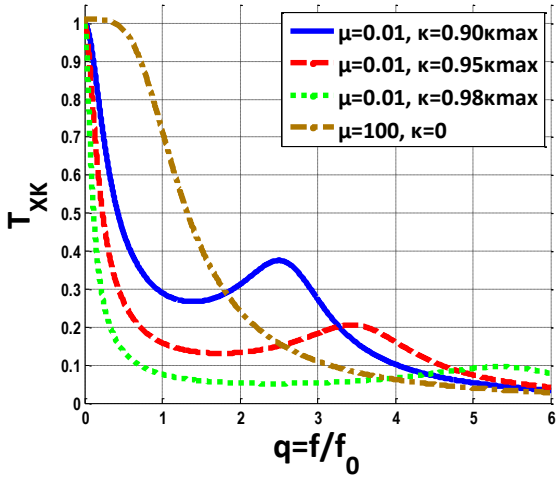

Figure 2.6: Transfer functions T_{XK} of the KDamper for values of κ , μ close to the limits.

Figure 2.5 presents the variation of ρ and $T_{XKI} = T_{XKL} = T_{XKR}$ with the increase of the parameter κ. Figure 2.6 presents Transfer functions for values of κ or μ close to the limits. Values of low μ/high κ characterize the KDamper, while values high μ/low κ can be indicative of an inerter. As it can be observed, very low values of the transfer function of the KDamper, can be reached, quite below unity. Moreover, these values can be achieved by an almost mar-

ginal value of $\mu=0.01$. This fact implies that the KDamper essentially does not require an additional mass m_D. Moreover, the Kdamper indicates a superior behavior at the very low frequency range.

A first implication of eq. (2.42) is that there exists a range of values of κ for which:

$$T_{XKL}(\kappa) = T_{XKL}(\kappa) < 1 \quad \text{for} \quad \kappa_{\text{MAX}} \geq \kappa \geq \kappa_{UN} \tag{2.43}$$

Eq. (2.43) implies that in this case, the values $T_{XKI}=T_{XKL}=T_{XKR}$ do no longer present the maximum values of T_{XK} since $T_{XK}(q=0)=1$. Among others, this fact complicates the procedures for the selection of ζ_D based on averaging the slopes of T_{XK} at the frequencies q_L, q_R , as it is the classical approach, proposed in (Den Hartog, 1956).
Furthermore, although equations (2.36) and (2.42) imply that by increasing κ the transfer function $T_{XKI}=T_{XKL}=T_{XKR}$ can be reduced almost to zero, increasing κ has a number of implications in the design of the KDamper. First, as it can be observed by equations (2.36.a) to (2.36.c), high stiffness values result. Figure 2.7 reflects this fact to the increase of the stiffness values k_N, k_P and especially k_S.

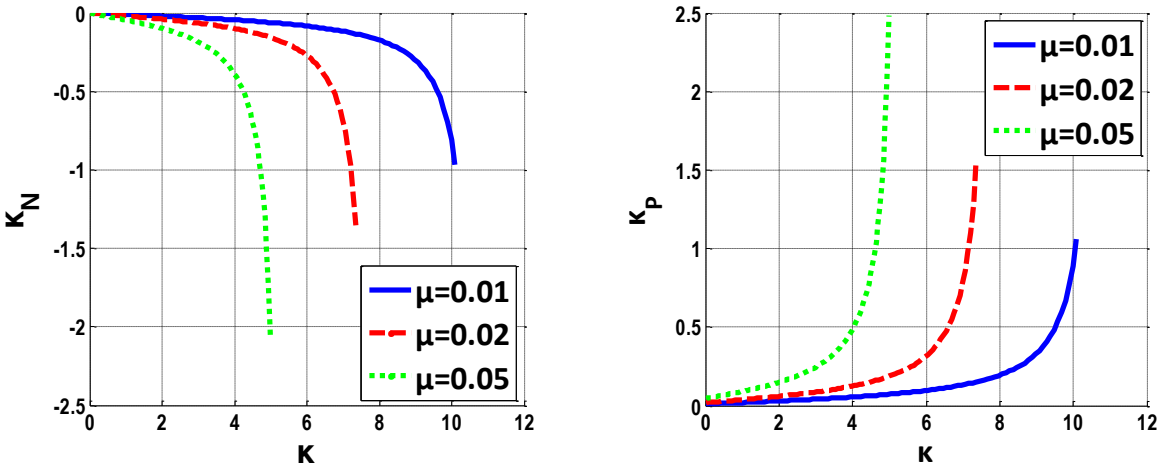

(a) (b)

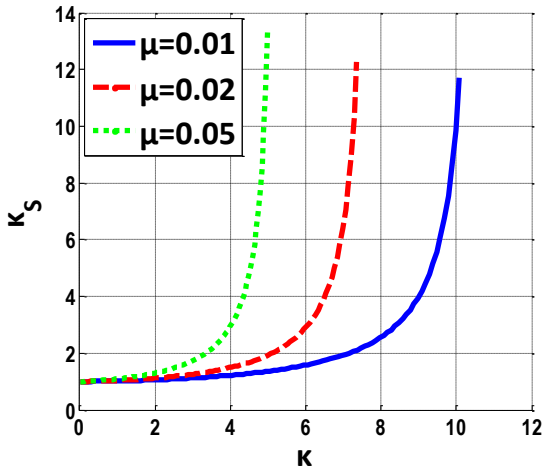

(c)

Figure 2.7: Increase of the values of the stiffness elements of the KDamper by the increase of κ. (a) κ_N, (b) κ_P, (c)κ_S.

Moreover, increasing the stiffness and especially k_N may endanger the static stability of the structure. Although theoretically the value of k_N is selected according to eq. (2.14) to ensure the static stability, variations of k_N result in practice due to various reasons, such as temperature variations, manufacturing tolerances, or non-linear behavior, since almost all negative stiffness designs result from unstable non-linear systems. Consequently, an increase of the absolute value of k_N by a factor ε may lead to a new value of k_{NL} where the structure becomes unstable:

$$k_S + \frac{k_P k_{NL}}{k_P + k_{NL}} = 0 \Leftrightarrow k_{NL} = -\frac{k_S k_P}{k_S + k_P} = (1+\varepsilon)k_N \tag{2.44}$$

Substitution of (2.36.a) to (2.36.c) into (2.44) leads to the following estimate for the static stability margin ε:

$$\varepsilon = \frac{1}{\kappa[(1+(1+\kappa)^2 \mu\rho^2]} \tag{2.45}$$

As it can be shown, the following PROPERTY 3 holds for ε.

PROPERTY 3: The increase of the negative stiffness of the system is upper bounded by the static stability limit of the structure:

$$\varepsilon \to 0 \quad \text{for} \quad \kappa \to \kappa_{MAX} \tag{2.46}$$

Figure 2.8 presents the variation of κ_{MAX} over μ and of ε over κ and μ.

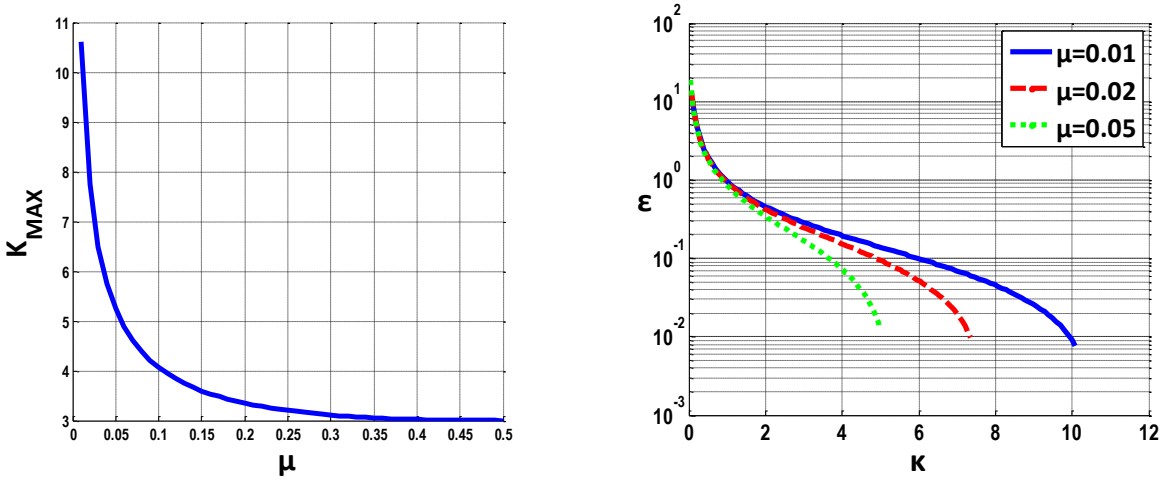

(a) (b)

Figure 2.8: *Variation of KDamper parameters a) Effect of the mass ratio μ on the maximum value κ_{MAX} of κ. b) Effect of κ and μ over the static stability margin ε.*

Finally, as it is observed from eq. (2.21.d), high values of κ result to increased amplitudes of the response y, which may encounter further technological constraints. For example, eq. (2.21.d) for $q=0$ leads to:

$$T_{YXK}(q=0) = \frac{Y(q=0)}{X(q=0)} = \frac{Y(q=0)}{X_{ST}} = 1+\kappa \tag{2.47}$$

3 THEORY AND MODELING

The wind turbine tower is modeled as an assemblage of beam elements with sway degrees of freedom considered to be the dynamic degrees of freedom. The theoretical development is based on the assumption that the cross-sectional dimension within the element remains the same, i.e. prismatic beam element. Additional assumptions made for the analytical formulation are: (i) the wind turbine tower is considered to remain within the elastic limit under the earthquake excitation and/or the aerodynamic loads; (ii) the system is subjected to a single horizontal (uni-directional) component of the earthquake ground motion; and (iii) the effects of soil-structure-interaction (SSI) are not taken into consideration.

3.1 Mathematical modeling of wind turbine tower

Figure 3.1(a–f) shows the lumped mass model of the wind turbine tower, placement of the TMDs and the KDamper and the degrees of freedom considered in the study. The governing equations of motion for the wind turbine tower installed with the STMD at the top and installed with the d-TMDs and the KDamper are obtained by considering the equilibrium of forces at the location of each degree of freedom as follows.

$$[M_S]\{\ddot{x}_S\}+[C_S]\{\dot{x}_S\}+[K_S]\{x_S\}=-[M_S]\{r\}\ddot{x}_g \tag{3.1.a}$$

$$[M_S]\{\ddot{x}_S\}+[C_S]\{\dot{x}_S\}+[K_S]\{x_S\}=[P] \tag{3.1.b}$$

where $[M_S]$, $[C_S]$ and $[K_S]$ are the mass, damping, and stiffness matrices of the wind turbine tower, respectively of order $(N+n)\times(N+n)$. Here, N indicates degrees of freedom (DOF) for the wind turbine tower and n indicates DOF for the STMD, 2TMDs or KDamper.

Further, $\left\{x_S\right\} = \left\{x_1, \mathrm{x}_2, \mathrm{x}_3, ..., \mathrm{x}_{N-1}, \mathrm{x}_N, \mathrm{X}_1, ..., \mathrm{X}_n\right\}^T$, $\left\{\dot{x}_s\right\}$ and $\left\{\ddot{x}_s\right\}$ are the unknown relative nodal displacement, velocity, and acceleration vectors, respectively. The earthquake ground acceleration is represented by $\ddot{x}_g$ and $\{r\}$ is the vector of influence coefficients. The modal frequencies and mode shapes of the wind turbine tower without control systems are determined by solving the Eigen value problem. A TMD is placed where the mode shape amplitude of the wind turbine tower is the largest/larger in a particular mode and is tuned to the corresponding modal frequency. Not more than one TMD is placed at a location, and the stiffness (ki) and damping (ci) parameters of the TMDs (i = 1. . .n) are calculated based on the modal frequencies. For the TMDs and the KDamper, the mass matrix is of order $(N+n)\times(N+n)$ as follows:

$$\left[M_S\right] = \begin{bmatrix} \left[M_N\right]_{N\times N} & \left[0\right]_{n\times N} \\ \left[0\right]_{n\times N} & \left[m_n\right]_{n\times n} \end{bmatrix}_{(N+n)\times(N+n)} \tag{3.2}$$

where $\left[M_N\right]_{N\times N}$ shows the mass matrix for the chimney and $\left[m_n\right]_{n\times n}$ indicates the mass matrix of the TMDs. In eq. (3.2), for obtaining mass matrix corresponding to the STMD n = 1 is considered. The condensed stiffness matrix $\left[K_N\right]_{N\times N}$ is corresponding to the sway degrees of freedom taken as the dynamic DOF. The damping matrix $\left[C_N\right]_{N\times N}$ is not explicitly known but is obtained with the help of the Rayleigh's approach using same damping ratio in all modes. The stiffness matrix, $\left[K_N\right]_{N\times N}$ and damping matrix, $\left[C_N\right]_{N\times N}$ are expressed corresponding to the degrees of freedom associated with the TMDs or the KDamper. For the wind turbine tower installed with the STMD, 2TMDs or KDamper stiffness and damping are inputs in the generic stiffness matrix $\left[K_S\right]$ and damping matrix $\left[C_S\right]$ as follows.

$$\left[K_S\right] = \begin{bmatrix} \begin{bmatrix} \left[K_N\right]_{N\times N} & \left[0\right]_{N\times n} \\ \left[0\right]_{n\times N} & \left[0\right]_{n\times n} \end{bmatrix} + \begin{bmatrix} \left[K_n\right]_{N\times N} & -\left[K_n\right]_{N\times n} \\ -\left[K_n\right]_{n\times N} & \left[K_n\right]_{n\times n} \end{bmatrix} \end{bmatrix}_{(N+n)\times(N+n)} \tag{3.3}$$

$$\left[C_S\right] = \begin{bmatrix} \begin{bmatrix} \left[C_N\right]_{N\times N} & \left[0\right]_{N\times n} \\ \left[0\right]_{n\times N} & \left[0\right]_{n\times n} \end{bmatrix} + \begin{bmatrix} \left[C_n\right]_{N\times N} & -\left[C_n\right]_{N\times n} \\ -\left[C_n\right]_{n\times N} & \left[C_n\right]_{n\times n} \end{bmatrix} \end{bmatrix}_{(N+n)\times(N+n)} \tag{3.4}$$

The coupled differential equations of motion (Eq. (3.1.a-b)) for the wind turbine tower installed with TMD(s) or KDamper are thus derived and solved using Newmark's integration method.

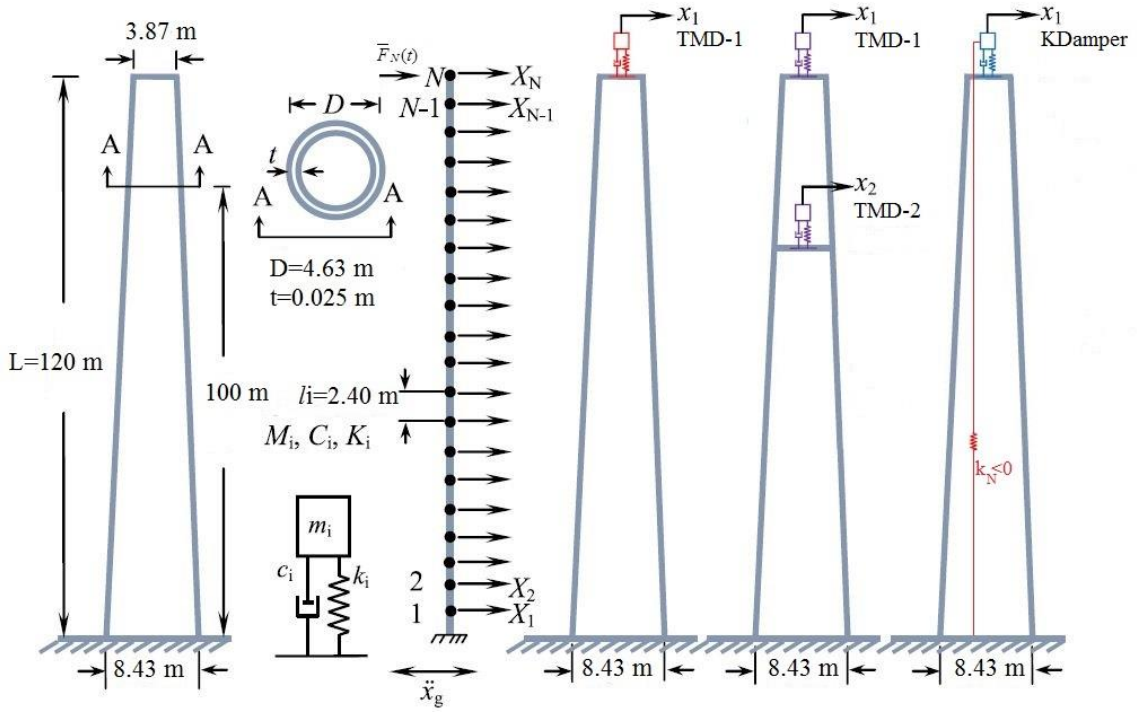

(a) (b) (c) (d) (e) (f)

Figure 3.1: Details of the wind turbine tower (a) with no-control, i.e. uncontrolled, (b) schematic diagram of TMD and section A-A, (c) lumped mass idealization for wind turbine tower installed with, (d) single TMD, (e) 2 TMDs, and (f) KDamper.

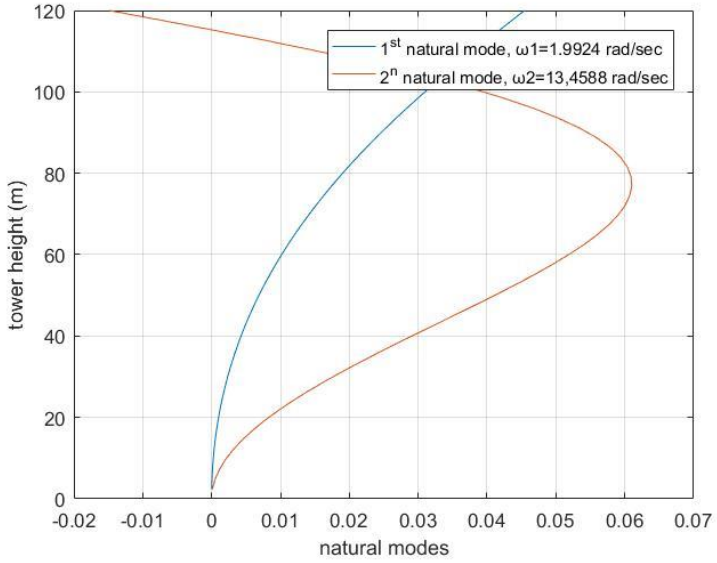

Figure 3.2: Modeshapes of wind turbine tower with fixed support.

3.2 Designing and placement of resonant dampers

3.2.1 Test case 1: Uncontrolled wind turbine tower

3.2.2 Test case 2: Single TMD placed on top of wind turbine tower

The deciding criterion for the use of the single TMD is the control of the first modal response. The frequency of the TMD is calculated as:

$$f = \frac{\omega}{\Omega_1} \tag{3.5}$$

where the tuning frequency ratio is $f = 1$. Here, ω and Ω_1 respectively are the frequency of the TMD and the first natural frequency of the wind turbine tower before controlling. The effectiveness of the TMD installed on a wind turbine tower depends on mass ratio, $\mu = m_t / M_t$, where m_t is the mass of the TMD, $M_t = \sum_{i=1}^{N} M_i$ is the mass of the wind turbine tower and M_i are the lumped masses of the wind turbine tower.
The stiffness k is used for adjusting the frequency of the TMD such that:

$$k = m_t \omega^2 \tag{3.6}$$

The damping c of the TMD is calculated as follows:

$$c = 2\zeta_D m_t \omega \tag{3.7}$$

where ζ_D is the damping ratio of the TMD.

The mass, stiffness and damping matrix of the TMD are calculated as follows:

$$[m_n]_{1x1} = [m_t] \tag{3.8}$$

$$[K_n]_{NxN} = \begin{bmatrix} 0 & \cdots & 0 \\ \vdots & \ddots & \vdots \\ 0 & \cdots & k \end{bmatrix} \tag{3.9.a}$$

$$[K_n]_{1xN} = [K_n]^T_{Nx1} = \begin{bmatrix} 0 & \cdots & k \end{bmatrix} \tag{3.9.b}$$

$$[K_n]_{1x1} = \begin{bmatrix} k \end{bmatrix} \tag{3.9.c}$$

$$[\mathrm{C}_n]_{NxN} = \begin{bmatrix} 0 & \cdots & 0 \\ \vdots & \ddots & \vdots \\ 0 & \cdots & c \end{bmatrix} \tag{3.9.a}$$

$$[\mathrm{C}_n]_{1xN} = [\mathrm{C}_n]^T_{Nx1} = \begin{bmatrix} 0 & \cdots & c \end{bmatrix} \tag{3.9.b}$$

$$[\mathrm{C}_n]_{1x1} = \begin{bmatrix} c \end{bmatrix} \tag{3.9.c}$$

Finally, the mass $[M_S]$, damping $[C_S]$, and stiffness $[K_S]$ matrices of the wind turbine tower are calculated with the following relations:

$$[M_S] = \begin{bmatrix} [M_N]_{N\times N} & [0]_{N\times 1} \\ [0]_{1\times N} & [m_n]_{1\times 1} \end{bmatrix}_{(N+1)\times(N+1)} \tag{3.2}$$

$$[K_S] = \begin{bmatrix} \begin{bmatrix} [K_N]_{N\times N} & [0]_{N\times 1} \\ [0]_{1\times N} & [0]_{1\times 1} \end{bmatrix} + \begin{bmatrix} [K_n]_{N\times N} & -[K_n]_{N\times 1} \\ -[K_n]_{1\times N} & [K_n]_{1\times 1} \end{bmatrix} \end{bmatrix}_{(N+1)\times(N+1)} \tag{3.3}$$

$$[C_S] = \begin{bmatrix} \begin{bmatrix} [C_N]_{N\times N} & [0]_{N\times 1} \\ [0]_{1\times N} & [0]_{1\times 1} \end{bmatrix} + \begin{bmatrix} [C_n]_{N\times N} & -[C_n]_{N\times 1} \\ -[C_n]_{1\times N} & [C_n]_{1\times 1} \end{bmatrix} \end{bmatrix}_{(N+1)\times(N+1)} \tag{3.4}$$

3.2.3 Test case 2(b): Pendulum placed at the top of wind turbine tower.

The procedure is the same with the single TMD placed on top of wind turbine tower, with the difference for the calculation of the stiffness K_{pend} (Eq. (23)).

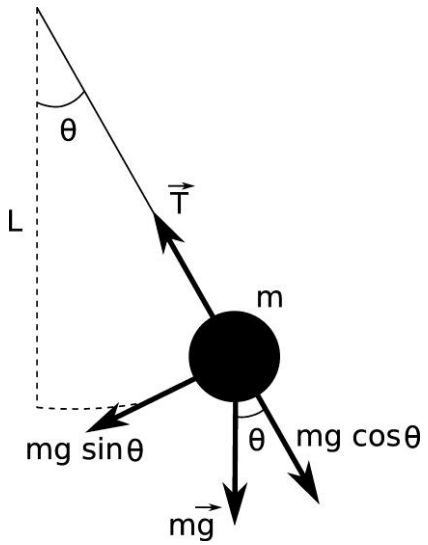

Figure 3.3: Simple Pendulum assuming linear behavior.

$$T = mg\cos\theta \tag{3.10.a}$$

$$T_x = T\sin\theta \tag{3.10.b}$$

$$T_x = mg\cos\theta\sin\theta = mg\sqrt{\left(\frac{u}{L}\right)^2 - \left(\frac{u}{L}\right)^4} \tag{3.10.c}$$

$$\theta << \quad \Rightarrow \cos\theta \approx 1,\ \theta \approx \sin\theta = u / \mathrm{L} \tag{3.10.d}$$

$$T_{x,linear} = mgu / L \tag{3.10.e}$$

Thus the stiffness and the damping of the pendulum is :

$$K_{pend} = \frac{\partial T_x}{\partial u} = mg / L \tag{3.11}$$

$$C_{pend} = 2\zeta_{pend}\sqrt{K_{pend} \cdot m} \tag{3.12}$$

And the mass, stiffness and damping matrix of the TMD-Pendulum are calculated as follows:

$$[m_n]_{1x1} = [m] \tag{3.13}$$

$$[K_n]_{NxN} = \begin{bmatrix} 0 & \cdots & 0 \\ \vdots & \ddots & \vdots \\ 0 & \cdots & K_{pend} \end{bmatrix} \tag{3.14.a}$$

$$[K_n]_{1xN} = [K_n]^T_{Nx1} = \begin{bmatrix} 0 & \cdots & K_{pend} \end{bmatrix} \tag{3.14.b}$$

$$[K_n]_{1x1} = \begin{bmatrix} K_{pend} \end{bmatrix} \tag{3.14.c}$$

$$[\mathrm{C}_n]_{NxN} = \begin{bmatrix} 0 & \cdots & 0 \\ \vdots & \ddots & \vdots \\ 0 & \cdots & C_{pend} \end{bmatrix} \tag{3.15.a}$$

$$[\mathrm{C}_n]_{1xN} = [\mathrm{C}_n]^T_{Nx1} = \begin{bmatrix} 0 & \cdots & C_{pend} \end{bmatrix} \tag{3.15.b}$$

$$[\mathrm{C}_n]_{1x1} = \begin{bmatrix} C_{pend} \end{bmatrix} \tag{3.15.c}$$

Finally, the mass $[M_S]$, damping $[C_S]$, and stiffness $[K_S]$ matrices of the wind turbine tower are calculated with the following relations:

$$[M_S]=\begin{bmatrix}[M_N]_{N\times N} & [0]_{N\times 1}\\ [0]_{1\times N} & [m_n]_{1\times 1}\end{bmatrix}_{(N+1)\times(N+1)} \tag{3.2}$$

$$[K_S]=\left[\begin{bmatrix}[K_N]_{N\times N} & [0]_{N\times 1}\\ [0]_{1\times N} & [0]_{1\times 1}\end{bmatrix}+\begin{bmatrix}[K_n]_{N\times N} & -[K_n]_{N\times 1}\\ -[K_n]_{1\times N} & [K_n]_{1\times 1}\end{bmatrix}\right]_{(N+1)\times(N+1)} \tag{3.3}$$

$$[C_S]=\left[\begin{bmatrix}[C_N]_{N\times N} & [0]_{N\times 1}\\ [0]_{1\times N} & [0]_{1\times 1}\end{bmatrix}+\begin{bmatrix}[C_n]_{N\times N} & -[C_n]_{N\times 1}\\ -[C_n]_{1\times N} & [C_n]_{1\times 1}\end{bmatrix}\right]_{(N+1)\times(N+1)} \tag{3.4}$$

3.2.4 Test case 3: 2TMDs placed according to the 2 first modal shapes.

This time the goal is to control the first 2 modal responses of the wind turbine tower. The frequency of each TMD is calculated as:

$$f_i=\frac{\omega_i}{\Omega_i} \quad \text{i=1,2} \tag{3.16}$$

where all (i=1,2) tuning frequency ratios are, $f_i=1$. Here, ω_i and Ω_i respectively are the frequencies of the TMD and natural frequencies of the wind turbine tower before controlling. The effectiveness of the TMD installed on a wind turbine tower depends on mass ratio, $\mu=m_t/M_t$, where $m_t=\sum_{i=1}^{2}m_i$ is the total mass of the TMDs, $M_t=\sum_{i=1}^{N}M_i$ is the mass of the wind turbine tower, m_i and M_i are the lumped masses of the TMDs and wind turbine tower, respectively. Thus, the mass of the TMDs is calculated by $m_t=\mu M_t$. The masses of the TMDs, $m_i=diag(m_1,m_2)$ are taken equal. Mass (m_i) used for each TMD unit is calculated as follows.

$$m_i=\frac{m_t}{2} \quad \text{i=1,2} \tag{3.17}$$

The stiffness (ki) is used for adjusting the frequency of each TMD unit such that

$$k_i = m_i \omega_i^2 \quad \text{i=1,2} \tag{3.18}$$

The damping ratio $(\zeta_D = \zeta_1 = \zeta_2)$ of the TMDs is kept the same and the damping (c_i) of the TMDs is calculated as follows:

$$c_i = 2\zeta_D m_i \omega_i \quad \text{i=1,2} \tag{3.19}$$

The first TMD that controls the first modal shape is placed at the top, where the first modal shape presents its maximum value. The second TMD is placed respectively where the 2nd modal shape presents its maximum value. Thus the mass, stiffness and damping matrix of the TMDs are calculated as follows:

$$[m_n]_{2x2} = \begin{bmatrix} m_1 & 0 \\ 0 & m_2 \end{bmatrix} \tag{3.20}$$

$$[K_n]_{NxN} = \begin{bmatrix} 0 & \cdots & 0 & \cdots & 0 \\ \vdots & [0] & \vdots & [0] & \vdots \\ 0 & \cdots & k_2 & \cdots & 0 \\ \vdots & [0] & \vdots & [0] & \vdots \\ 0 & \cdots & 0 & \cdots & k_1 \end{bmatrix} \tag{3.21.a}$$

$$[K_n]_{2xN} = [K_n]^T_{Nx2} = \begin{bmatrix} 0 & \cdots & 0 & \cdots & k_1 \\ 0 & \cdots & k_2 & \cdots & 0 \end{bmatrix} \tag{3.21.b}$$

$$[K_n]_{2x2} = \begin{bmatrix} k_1 & 0 \\ 0 & k_2 \end{bmatrix} \tag{3.21.c}$$

$$[C_n]_{NxN} = \begin{bmatrix} 0 & \cdots & 0 & \cdots & 0 \\ \vdots & [0] & \vdots & [0] & \vdots \\ 0 & \cdots & c_2 & \cdots & 0 \\ \vdots & [0] & \vdots & [0] & \vdots \\ 0 & \cdots & 0 & \cdots & c_1 \end{bmatrix} \tag{3.22.a}$$

$$[\mathrm{C}_n]_{2xN} = [\mathrm{C}_n]^T_{Nx2} = \begin{bmatrix} 0 & \cdots & 0 & \cdots & c_1 \\ 0 & \cdots & c_2 & \cdots & 0 \end{bmatrix} \tag{3.22.b}$$

$$[\mathrm{C}_n]_{2x2} = \begin{bmatrix} c_1 & 0 \\ 0 & c_2 \end{bmatrix} \tag{3.22.c}$$

Finally, the mass $[M_S]$, damping $[C_S]$, and stiffness $[K_S]$ matrices of the wind turbine tower are calculated with the following relations:

$$[M_S] = \begin{bmatrix} [M_N]_{N\times N} & [0]_{N\times 2} \\ [0]_{2\times N} & [m_n]_{2\times 2} \end{bmatrix}_{(N+2)\times(N+2)} \tag{3.2}$$

$$[K_S] = \left[\begin{bmatrix} [K_N]_{N\times N} & [0]_{N\times 2} \\ [0]_{2\times N} & [0]_{2\times 2} \end{bmatrix} + \begin{bmatrix} [K_n]_{N\times N} & -[K_n]_{N\times 2} \\ -[K_n]_{2\times N} & [K_n]_{2\times 2} \end{bmatrix} \right]_{(N+2)\times(N+2)} \tag{3.3}$$

$$[C_S] = \left[\begin{bmatrix} [C_N]_{N\times N} & [0]_{N\times 2} \\ [0]_{2\times N} & [0]_{2\times 2} \end{bmatrix} + \begin{bmatrix} [C_n]_{N\times N} & -[C_n]_{N\times 2} \\ -[C_n]_{2\times N} & [C_n]_{2\times 2} \end{bmatrix} \right]_{(N+2)\times(N+2)} \tag{3.4}$$

3.2.5 Test case 4: TMD using as its additional mass the existing concentrated mass at the top of wind turbine tower, m_{top}.

In this test case the mass of the TMD is constant and has the value m_{top}. The stiffness k is not explicit knows as in the previews test cases that it was used for adjusting the frequency of the TMD with a natural frequency of the wind turbine before control. The damping c of the TMD is calculated as follows:

$$c = 2\zeta_D \sqrt{k \cdot m_{top}} \tag{3.23}$$

where ζ_D is the damping ratio of the TMD.

The mass, stiffness and damping matrix of the TMD are calculated as follows:

$$[m_n]_{1x1} = \left[m_{top} \right] \tag{3.24}$$

$$[K_n]_{NxN} = \begin{bmatrix} 0 & \cdots & 0 \\ \vdots & \ddots & \vdots \\ 0 & \cdots & k \end{bmatrix} \tag{3.25.a}$$

$$[K_n]_{1xN} = [K_n]^T_{Nx1} = \begin{bmatrix} 0 & \cdots & k \end{bmatrix} \tag{3.25.b}$$

$$[K_n]_{1x1} = \left[k \right] \tag{3.25.c}$$

$$[\mathrm{C}_n]_{NxN} = \begin{bmatrix} 0 & \cdots & 0 \\ \vdots & \ddots & \vdots \\ 0 & \cdots & c \end{bmatrix} \tag{3.26.a}$$

$$[\mathrm{C}_n]_{1xN} = [\mathrm{C}_n]^T_{Nx1} = \begin{bmatrix} 0 & \cdots & c \end{bmatrix} \tag{3.26.b}$$

$$[\mathrm{C}_n]_{1x1} = \left[c \right] \tag{3.26.c}$$

Finally, the mass $\left[M_S \right]$, damping $\left[C_S \right]$, and stiffness $\left[K_S \right]$ matrices of the wind turbine tower are calculated with the following relations:

$$\left[M_S \right] = \begin{bmatrix} \left[M_N \right]_{N \times N} & \left[0 \right]_{N \times 1} \\ \left[0 \right]_{1 \times N} & \left[m_n \right]_{1 \times 1} \end{bmatrix}_{(N+1) \times (N+1)} \tag{3.2}$$

$$\left[K_S \right] = \left[\begin{bmatrix} \left[K_N \right]_{N \times N} & \left[0 \right]_{N \times 1} \\ \left[0 \right]_{1 \times N} & \left[0 \right]_{1 \times 1} \end{bmatrix} + \begin{bmatrix} \left[K_n \right]_{N \times N} & -\left[K_n \right]_{N \times 1} \\ -\left[K_n \right]_{1 \times N} & \left[K_n \right]_{1 \times 1} \end{bmatrix} \right]_{(N+1) \times (N+1)} \tag{3.3}$$

$$[C_S]=\left[\begin{bmatrix}[C_N]_{N\times N} & [0]_{N\times 1}\\ [0]_{1\times N} & [0]_{1\times 1}\end{bmatrix}+\begin{bmatrix}[C_n]_{N\times N} & -[C_n]_{N\times 1}\\ -[C_n]_{1\times N} & [C_n]_{1\times 1}\end{bmatrix}\right]_{(N+1)\times(N+1)} \tag{3.4}$$

3.2.6 Test case 5: Single KDamper placed on top of the wind turbine tower.

The wind turbine tower is a continuum system and is modeled as an assemblage of beam elements with sway degrees of freedom considered to be the dynamic degrees of freedom, so it is a multi degree of freedom system therefore we cannot use the methodology that is described in the 2.4 so all 4 systems coefficients are unknown parameters of the system and are expressed:

Mass parameter: m_D

Positive stiffness element: k_e

Negative stiffness element: k_N

Damping: $c_D = 2\zeta_D\sqrt{(k_e + k_N)m_D}$

After the definition of the KDamper system parameters, the mass, stiffness and damping matrix of the KDamper are calculated as follows:

$$[m_n]_{1x1} = [m_D] \tag{3.27}$$

$$[K_n]_{NxN} = \begin{bmatrix} 0 & \cdots & 0 \\ \vdots & \ddots & \vdots \\ 0 & \cdots & k_e \end{bmatrix} \tag{3.28.a}$$

$$[K_n]_{1xN} = [K_n]^T_{Nx1} = [0 \quad \cdots \quad k_e] \tag{3.28.b}$$

$$[K_n]_{1x1} = [k_e + k_N] \tag{3.28.c}$$

$$[\mathrm{C}_n]_{NxN} = \begin{bmatrix} 0 & \cdots & 0 \\ \vdots & \ddots & \vdots \\ 0 & \cdots & c_D \end{bmatrix} \tag{3.29.a}$$

$$[\mathrm{C}_n]_{1xN} = [\mathrm{C}_n]^T_{Nx1} = \begin{bmatrix} 0 & \cdots & c_D \end{bmatrix} \tag{3.29.b}$$

$$[\mathrm{C}_n]_{1x1} = \begin{bmatrix} c_D \end{bmatrix} \tag{3.29.c}$$

Finally, the mass $[M_S]$, damping $[C_S]$, and stiffness $[K_S]$ matrices of the wind turbine tower are calculated with the following relations:

$$[M_S] = \begin{bmatrix} [M_N]_{N\times N} & [0]_{N\times 1} \\ [0]_{1\times N} & [m_n]_{1\times 1} \end{bmatrix}_{(N+1)\times(N+1)} \tag{3.2}$$

$$[K_S] = \left[\begin{bmatrix} [K_N]_{N\times N} & [0]_{N\times 1} \\ [0]_{1\times N} & [0]_{1\times 1} \end{bmatrix} + \begin{bmatrix} [K_n]_{N\times N} & -[K_n]_{N\times 1} \\ -[K_n]_{1\times N} & [K_n]_{1\times 1} \end{bmatrix} \right]_{(N+1)\times(N+1)} \tag{3.3}$$

$$[C_S] = \left[\begin{bmatrix} [C_N]_{N\times N} & [0]_{N\times 1} \\ [0]_{1\times N} & [0]_{1\times 1} \end{bmatrix} + \begin{bmatrix} [C_n]_{N\times N} & -[C_n]_{N\times 1} \\ -[C_n]_{1\times N} & [C_n]_{1\times 1} \end{bmatrix} \right]_{(N+1)\times(N+1)} \tag{3.4}$$

4 NUMERICAL STUDY ON WIND TURBINE TOWER

A wind turbine tower of variable tubular cross section ($E = 2.1\times10^{8}\ kN/m^{2}$, $\rho = 8.5\ tn/m^{3}$, $\nu = 0.3$, $G = 8.0769\times10^{7}\ kN/m^{2}$, $l = 120\ m$) supporting the NREL baseline 5-MW nacelle and rotor (3 blades of length $r_{bl} = 61.5\ m$) is examined. The radius and the thickness of the tubular cross section vary linearly along the tower length according to the dimensions. In order to take into account the inertial forces applied by the mechanical parts (nacelle, rotor and blades), an additional concentrated mass $m_{top} = 403.22\ tn$ is added at the top of the tower.

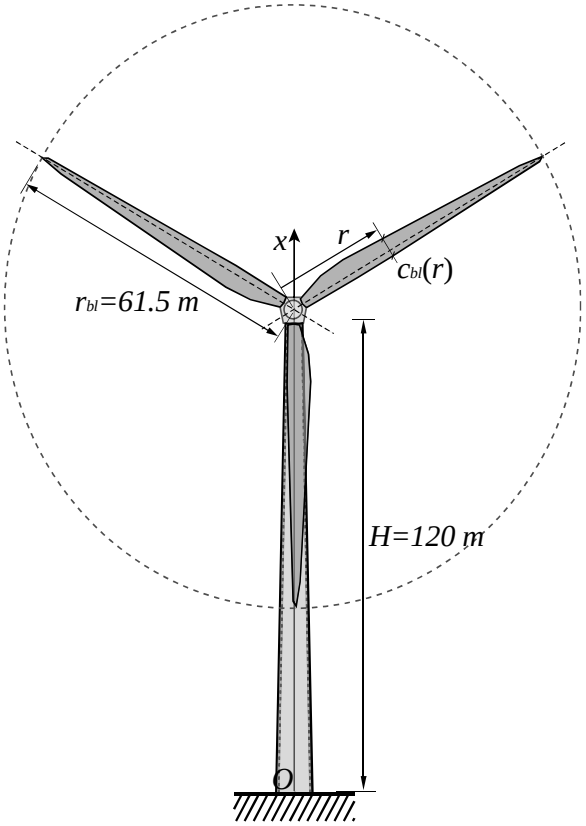

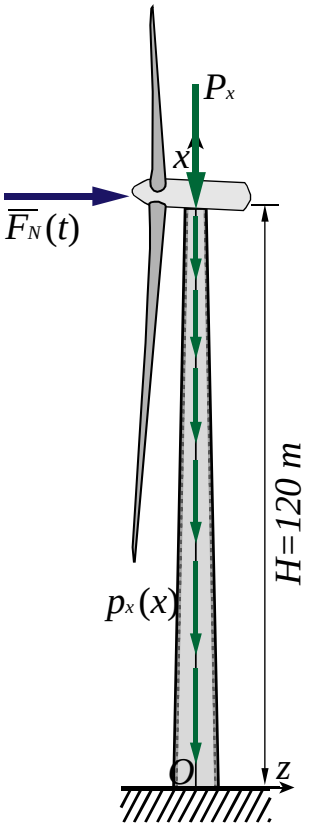

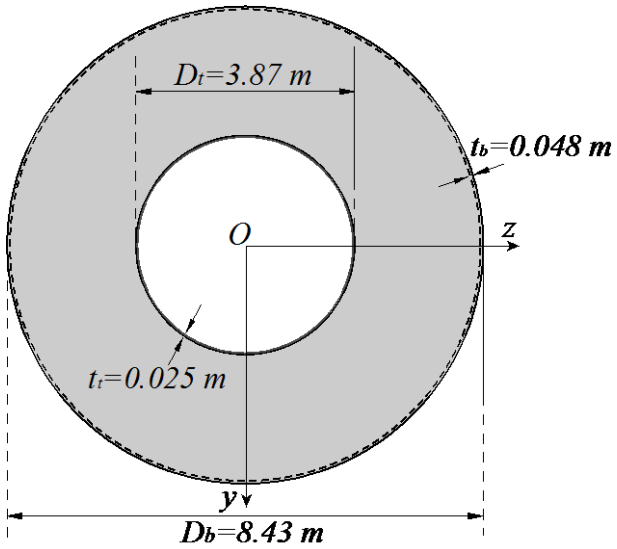

Figure 4.1: Front view, side view and floor plan of the wind turbine.

The tower is considered to be clamped at its base and is subjected to the seismic excitations of JMA (1995) and TABAS and to the time-dependent horizontal force $\overline{F}_N(t)$ at its top due to the wind.

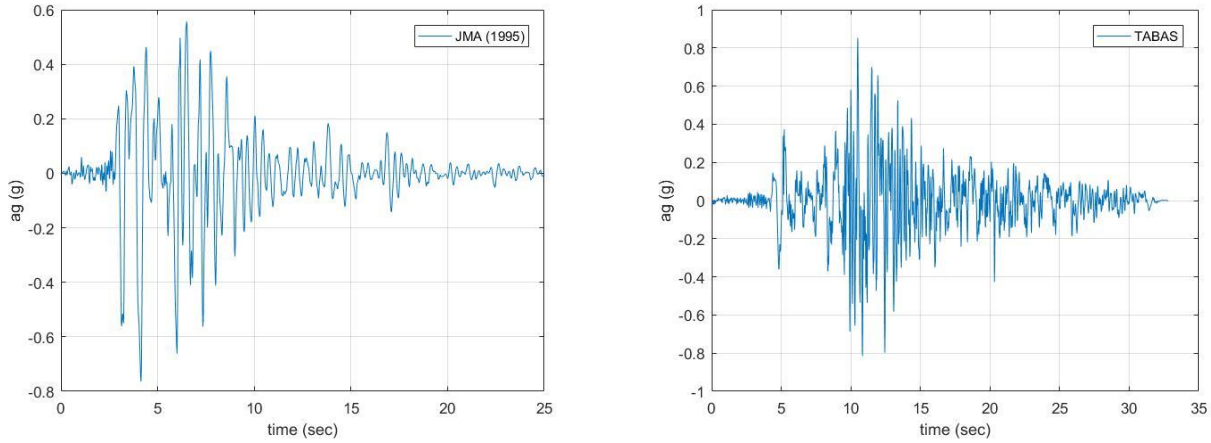

(a) (b)

Figure 4.2: JMA(1995) (a) and TABAS (b) excitation motion accelerograms.

Moreover, the force $\overline{F}_N(t)$ can be obtained by the following relation :

$$F_N(\mathrm{r},\mathrm{t}) = \frac{1}{2}\rho_{air} C_N(r) c_{bl}(r)(\overline{V}(t))^2 \tag{4.1}$$

where $\rho_{air} = 1.225\times10^{-3}\ tn/m^3$ is the air density and $C_N(r)$ is the coefficient computed by the corresponding lift $C_L(r)$ and drag $C_D(r)$ coefficients. The values of the latter coefficients depend on the airfoil characteristics of the blades and their distribution with respect to the "angle of attack" of the wind velocity $\overline{V}(t)$ vector passing through the blade profile can be retrieved from. It is noted that $\overline{V}(t)$ is assumed to have a uniform spatial distribution over the actuator disc. $c_{bl}(r)$ is the chord of the blade profile varying along the blade length *r*. In order to evaluate $C_N(r)$, the classical Blade Element Momentum theory is employed with an assumption of constant angular velocity of the blades $\Omega_{bl} = 12.1\ rpm$. Subsequently, breaking $\overline{V}(t)$ down into a mean component V_m and a fluctuating component $V(t)$, the corresponding mean and fluctuating components of $\overline{F}_N(t)$ can be obtained as

$$F_{Nm} = \frac{1}{2}\rho_{air} C_N(r) c_{bl}(r) V_m^2 \tag{4.2}$$

$$F_N(r,t) = \frac{1}{2}\rho_{air} C_N(r) c_{bl}(r)(2V_m V(t) + V(t)^2) \tag{4.3}$$

In this application the mean velocity is $V_m = 27\ m/\sec$.Moreover, in order to take into account the wind velocity fluctuation at the altitude of $l = 120\ m$, an artificial velocity time history is generated following the regulations of EC1, part1.4 with a standard deviation $\sigma = 3.3\ m/\sec$. After having established $F_N(\mathrm{r},\mathrm{t})$, the total concentrated force exerted on the top of the tower can be computed as

$$\overline{F}_N(t) = 3\int_0^{r_{bl}} \overline{F}_N(r,t)dr \tag{4.4}$$

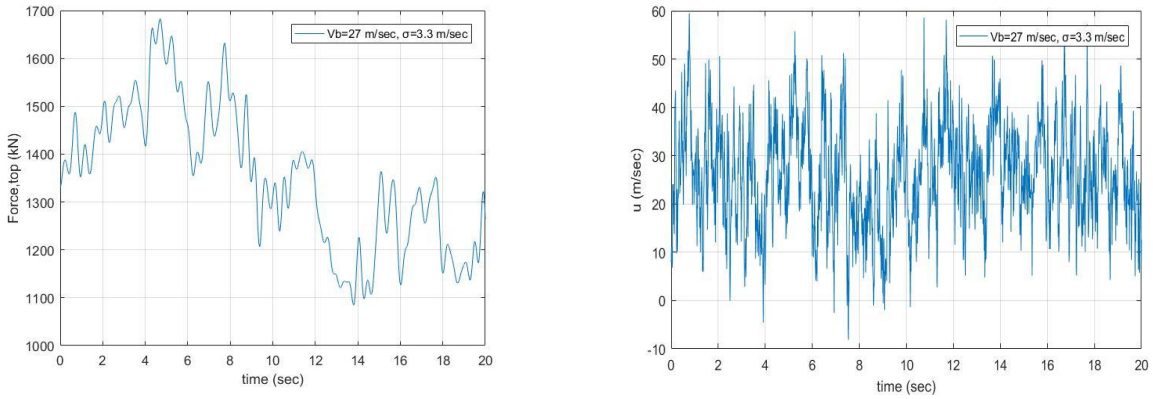

(a) (b)

Figure 4.3: (a) Time history of the total Force $\overline{F}_N(t)$ applied at the top of the tower and (b) basic velocity V_b at the altitude of 10 *m*.

4.1 Numerical results

4.1.1 Test case 1: uncontrolled wind turbine tower

The critical factor for the design of the wind turbine is the deflection at the top of the wind turbine tower. In Figure 4.4 are presented the transfer functions for the displacement at the top of the wind turbine tower for base excitation and input force at the top of the tower respectively.

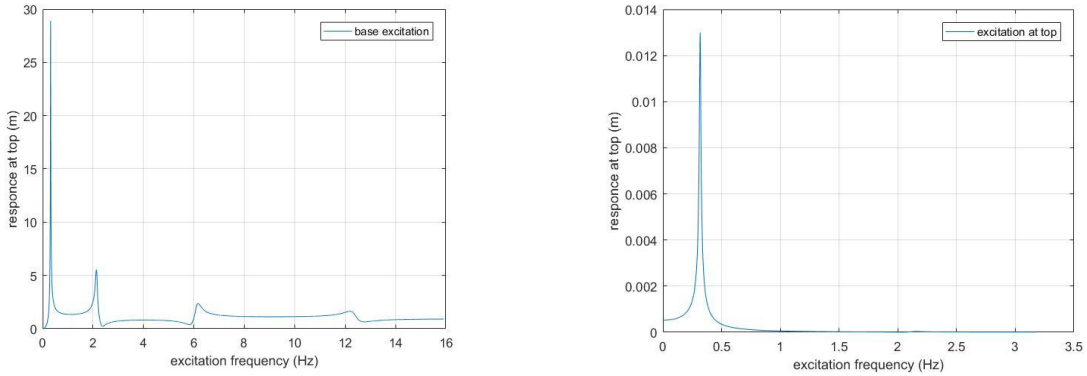

(a) (b)

Figure 4.4: Transfer function for the displacement at the top of the wind turbine tower due to (a) base excitation, and (b) excitation at top.

The Fourier transformations for the seismic excitation of JMA (1995) and TABAS and for the time-dependent horizontal force $\overline{F}_N(t)$ at its top due to the wind, are formulated so the main frequencies that are applied to the wind turbine can be determined.

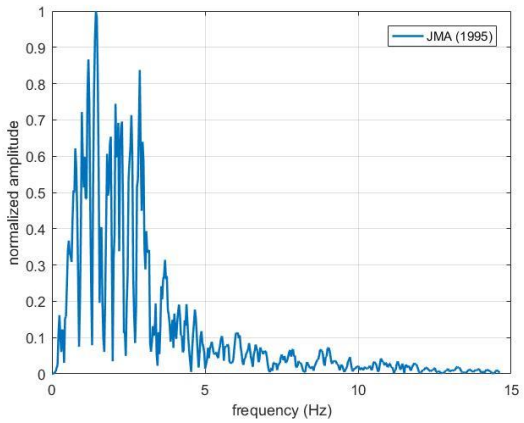

(a)

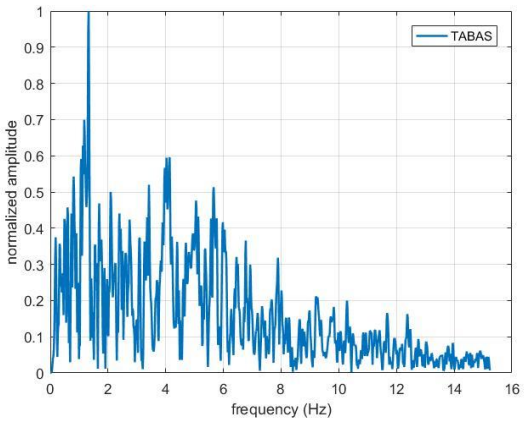

(b)

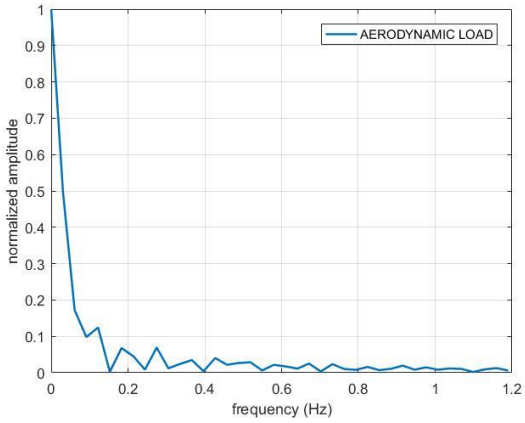

(c)

Figure 4.5: Fourier Transformation for (a) the seismic excitation of JMA (1995), (b) the seismic excitation of TABAS, and (c) for the time-dependent horizontal force $\overline{F}_N(t)$.

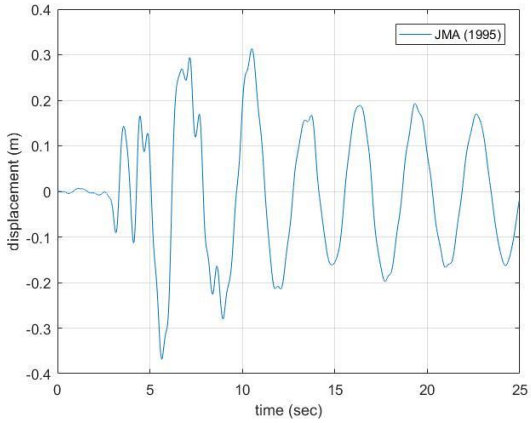

(a)

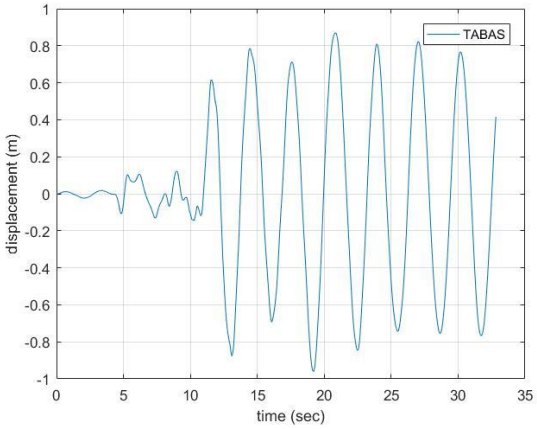

(b)

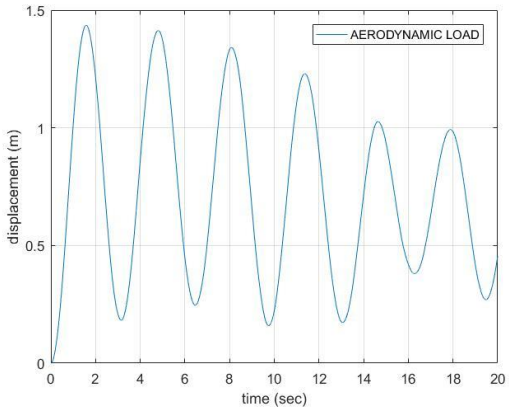

(c)

Figure 4.6: Dynamic response of the top of the wind turbine tower, displacement in (m), for (a) JMA (1995) seismic excitation ($\max\left|u_{top}\right| = 0.3682\ \ m$) , (b) TABAS seismic excitation ($\max\left|u_{top}\right| = 0.9607\ \ m$) and (c) the force $\overline{F}_N(t)$ due to the wind ($\max\left|u_{top}\right| = 1.436\ \ m$).

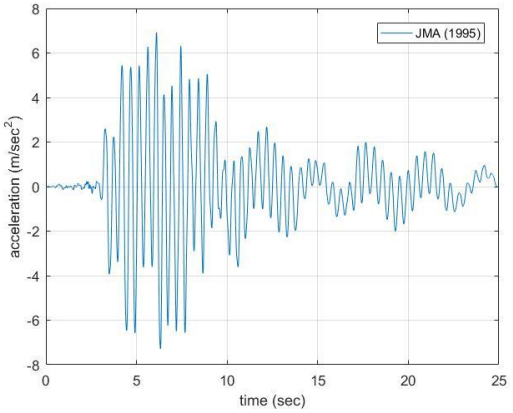

(a)

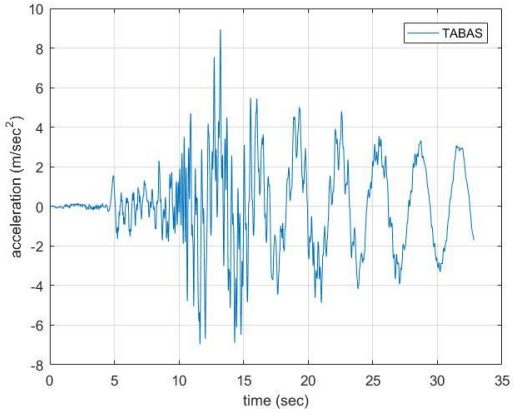

(b)

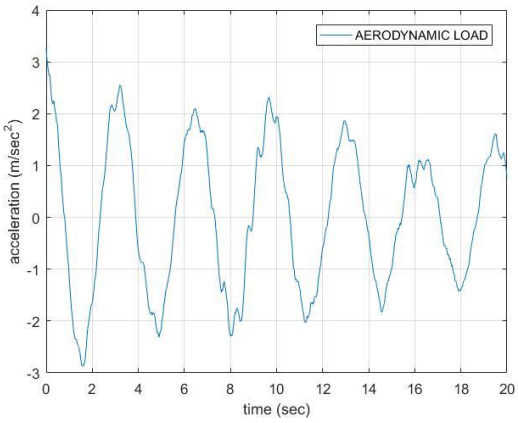

(c)

Figure 4.7: Dynamic response of the top of the wind turbine tower, acceleration in (m/sec^2), for (a) JMA (1995) seismic excitation ($\max\left|a_{top}\right| = 7.2802\ \ m/\sec^2$), (b) TABAS seismic excitation ($\max\left|a_{top}\right| = 8.9502\ \ m/\sec^2$) and (c) the force $\overline{F}_N(t)$ due to the wind ($\max\left|a_{top}\right| = 3.2665\ \ m/\sec^2$).

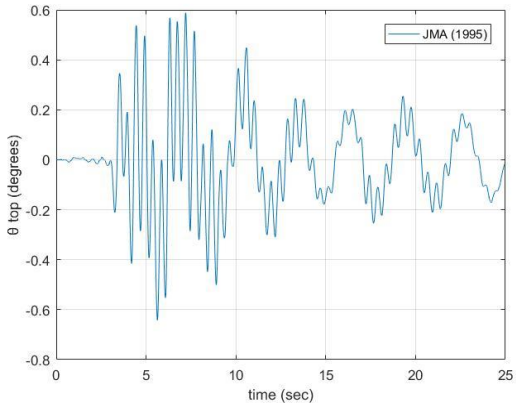

(a)

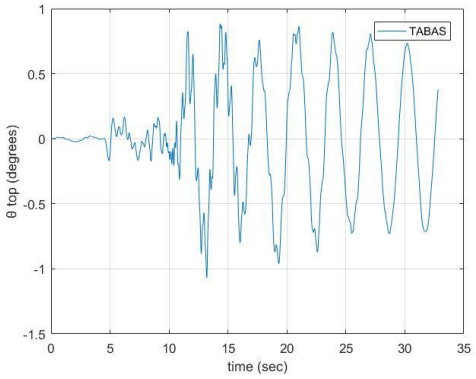

(b)

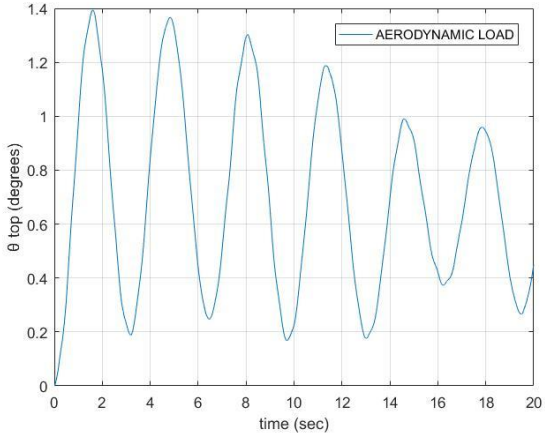

(c)

Figure 4.8: Dynamic response of the top of the wind turbine tower, acceleration in (m/sec^2), for (a) JMA (1995) seismic excitation ($\max\left|a_{top}\right| = 7.2802\ \ m/\sec^2$), (b) TABAS seismic excitation ($\max\left|a_{top}\right| = 8.9502\ \ m/\sec^2$) and (c) the force $\overline{F}_N(t)$ due to the wind ($\max\left|a_{top}\right| = 3.2665\ \ m/\sec^2$).

4.1.2 Test case 2: Single TMD placed on top of wind turbine tower – linear pendulum

Given that the TMD is tuned with the first natural frequency before control, the only parameter of the TMD is the mass ratio μ, the damping ratio is taken ζ=15%.

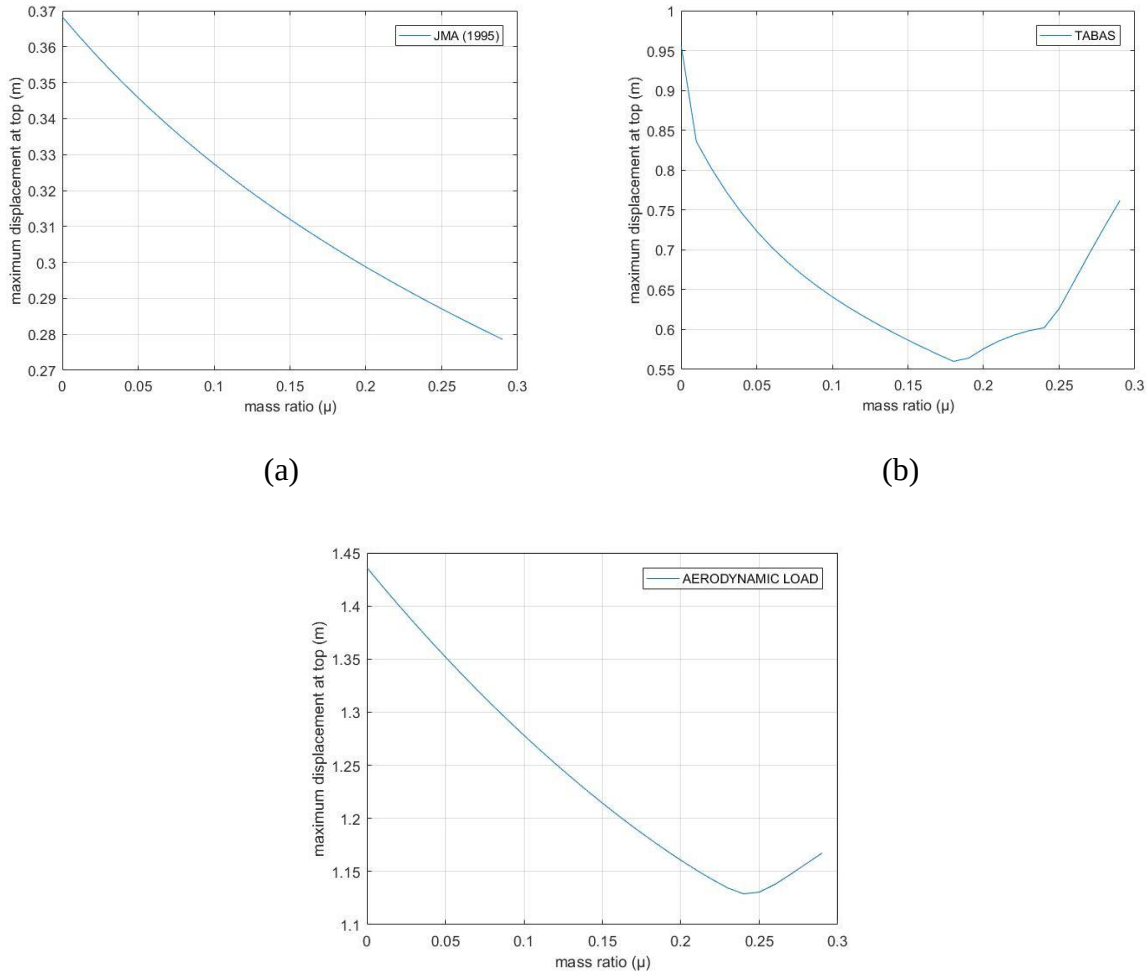

(a) (b)

(c)

Figure 4.9: Variation of the maximum displacement at the top of the wind turbine tower on the mass ratio μ for (a) seismic excitation of JMA (1995), (b) seismic excitation of TABAS, and (c) the force $\overline{F}_N(t)$ due to the wind.

For each of these excitations a verification is made in order to verify that the tuning of the TMD with the first natural frequency is optimum. A constant mass ratio of 10% and a damping ratio of 15% are taken and the only parameter is *Kd*. Figure 4.10 shows the maximum displacement at the top of the wind turbine tower in relation to *Kd*.

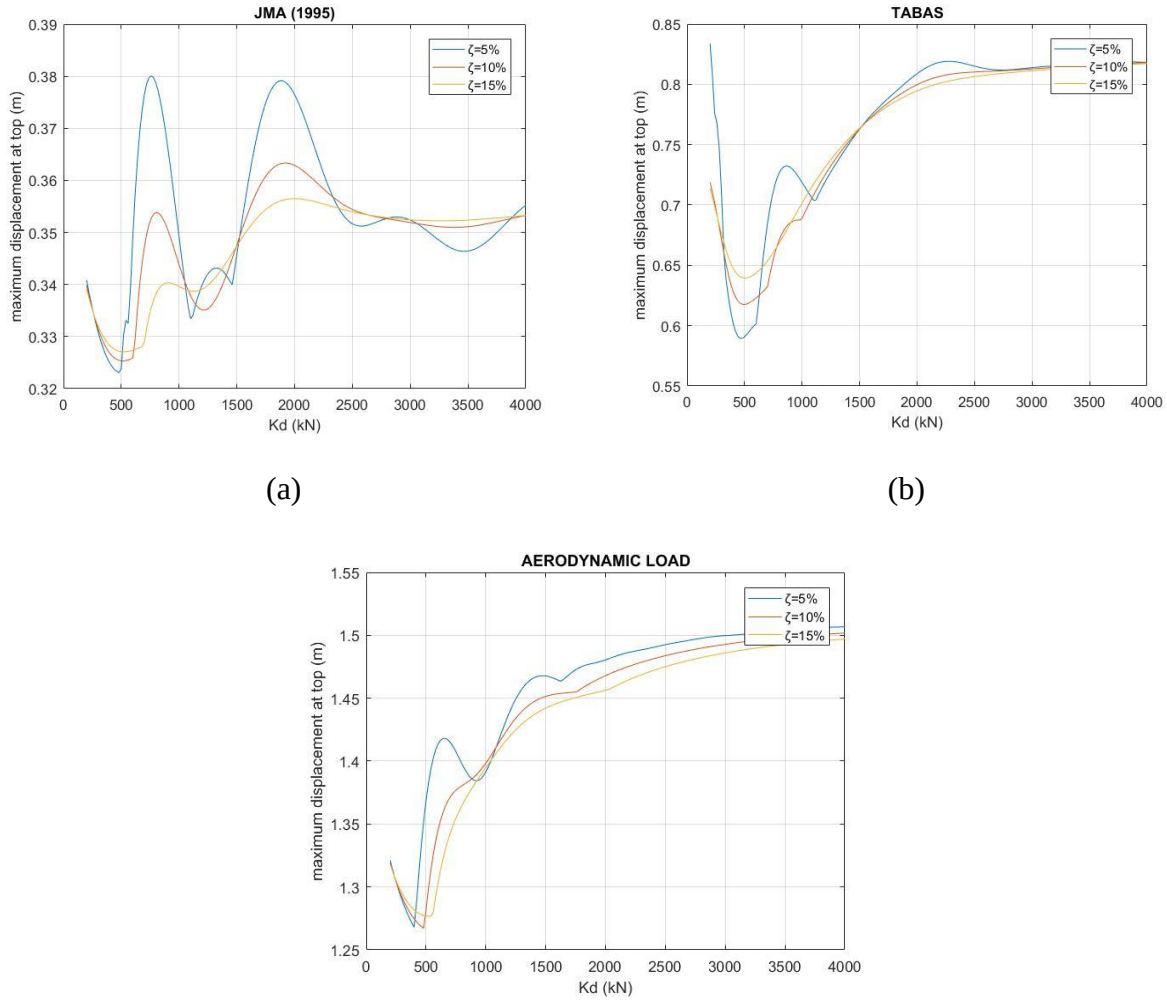

Figure 4.10: Variation of the maximum displacement at the top of the wind turbine tower on the stiffness *k* of the TMD.

Given that $\omega_1 = 1.9924\ rad/\sec$ the expected value for k is $k = \mu M_t \omega_1^2 = 454.3\ kN$ .It is observed that the minimum displacement of the top is around the value 450 *kN*.

Figure 4.11 shows the Transfer function for the wind turbine tower controlled with a TMD with a mass ratio of 10% and a damping ratio of 15%.

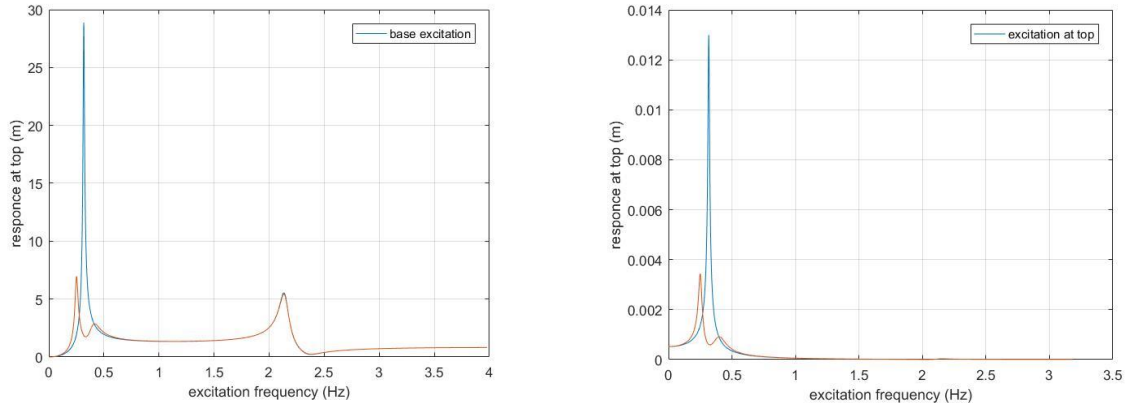

(a) (b)

Figure 4.11: Transfer function for the displacement at the top of the wind turbine tower, controlled with a TMD, due to (a) base excitation, and (b) excitation at top

Furthermore, a critical factor for the design of the wind turbine tower controlled with a TMD, is the relative displacement between the TMD and the top of the wind turbine tower for constructional reasons. The maximum displacement that the TMD can have, is 3,87/2=1.935 m.

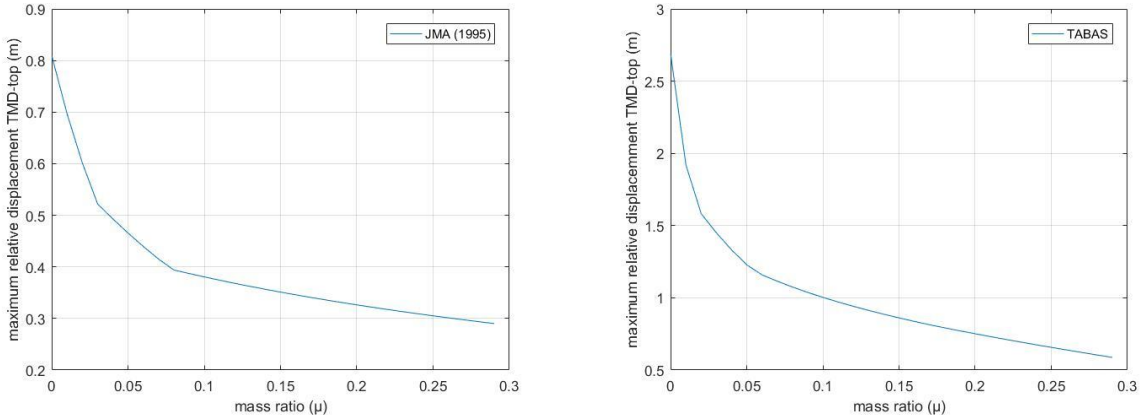

(a) (b)

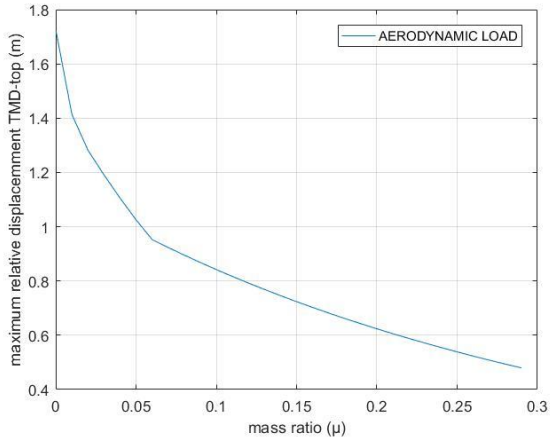

(c)

Figure 4.12: Variation of the maximum relative displacement of the TMD and the top of the wind turbine tower on the mass ratio μ.

In Table 4.1 are presented the optimum results after the implementation of a tuned TMD with a mass ratio of 10% and a damping ratio of 15%.

Table 4.1: Results after the implementation of a TMD of a mass ratio of 10% and a damping ratio of 15%.

Excitation	$\max\left\|u_{top}\right\|\ (m)$	$\max\left\|u_{relativeTMD}\right\|\ (m)$
JMA (1995)	0.3273	0.3807
TABAS	0.6408	1.0029
$\overline{F}_N(t)$	1.2783	0.8421

The implementation of the TMD leads to a new system with reduced displacements along the tower of the wind turbine and higher damping ratio. In order to calculate the exact value of the new damping ratio, the isolated system is subjected to a free vibration with initial conditions, which in this case are according to the first modal eigenform of the wind turbine tower before control with the initial condition of the TMD equal to the initial condition at the top of the wind turbine tower. More specifically, the value of the new damping ratio is calculated as:

$$\ln\left[\frac{u_{top}(t)}{u_{top}(t+T)}\right]=\frac{2\pi\zeta}{\sqrt{1-\zeta^2}} \tag{4.5}$$

where *T* is the time between two consecutive peaks of the dynamic response of the system, as shown in Figure 4.13 . The new damping ratio of the system equals to 15.68%.

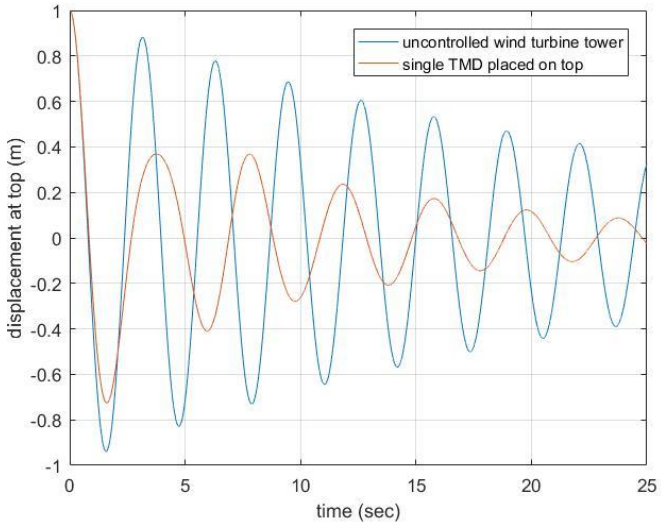

Figure 4.13: Dynamic response of the isolated system, with the TMD, to a free vibration with initial conditions.

4.1.3 Test case 3: 2 TMDs placed according to the 2 first modal shapes

Following the procedure that is presented in 3.1.4 the unknown parameter is the mass ratio μ, the damping ratio ζ is taken 15%. Again, beside the maximum displacement at the top of the wind turbine tower, a critical factor for the design of the wind turbine tower controlled with 2TMDs, is the relative displacements between the TMDs and the degree of freedom of the wind turbine tower that is relative with the respective TMD, for constructional reasons. The maximum displacement that can have a TMD is 3,87/2=1.935 m.

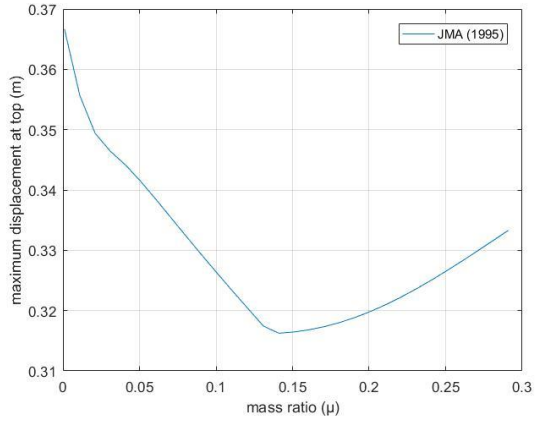

(a)

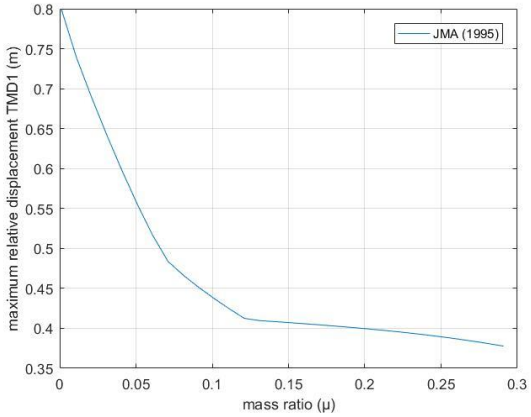

(b)

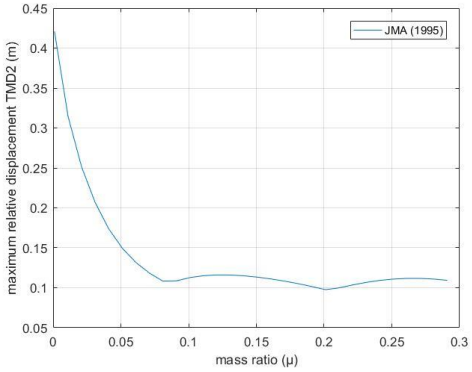

(c)

Figure 4.14: Variation of (a) the maximum displacement at the top of the wind turbine tower, (b) the maximum relative displacement of the TMD1, and (c) the maximum relative displacement of the TMD2 on the mass ratio μ for the seismic excitation of JMA (1995).

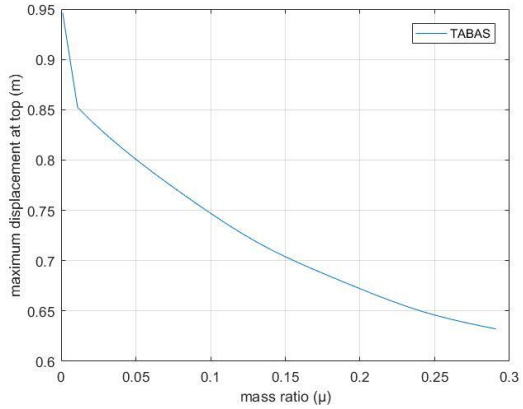

(a)

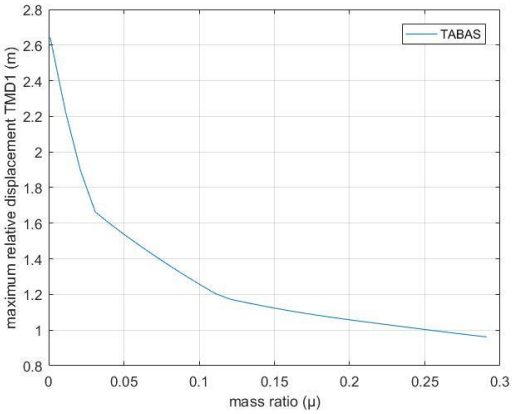

(b)

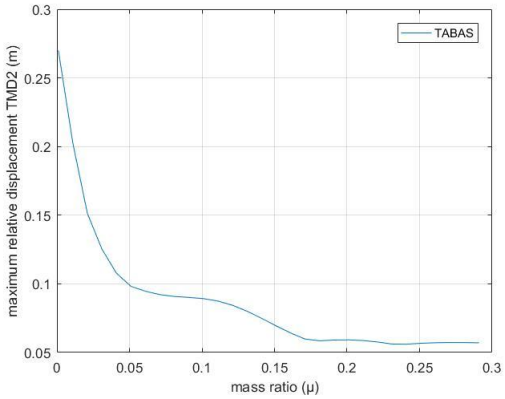

(c)

Figure 4.15: Variation of (a) the maximum displacement at the top of the wind turbine tower, (b) the maximum relative displacement of the TMD1, and (c) the maximum relative displacement of the TMD2 on the mass ratio μ for the seismic excitation of TABAS.

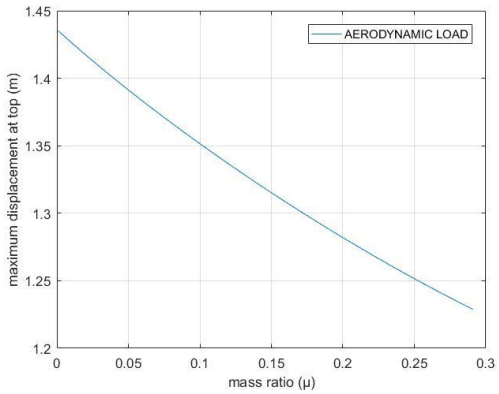

(a)

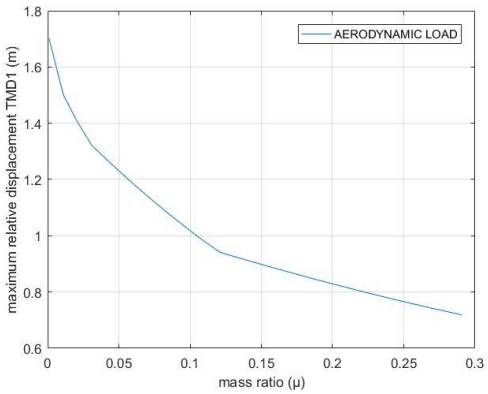

(b)

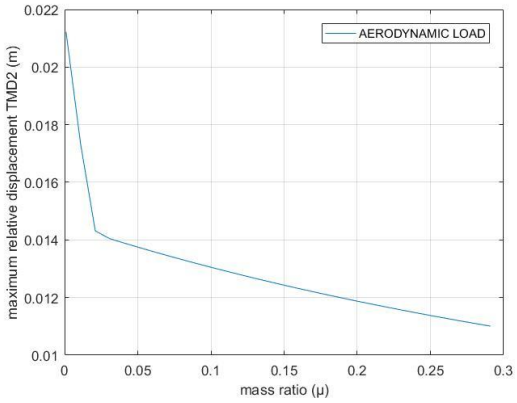

(c)

Figure 4.16: Variation of (a) the maximum displacement at the top of the wind turbine tower, (b) the maximum relative displacement of the TMD1, and (c) the maximum relative displacement of the TMD2 on the mass ratio μ for the force $\overline{F}_N(t)$ due to the wind.

In Figure 4.17 is shown the Transfer function for the wind turbine tower with 2TMDs controlling the first 2 natural frequencies of the wind turbine tower before control, with a mass ratio of 10% and a damping ratio of 15%.

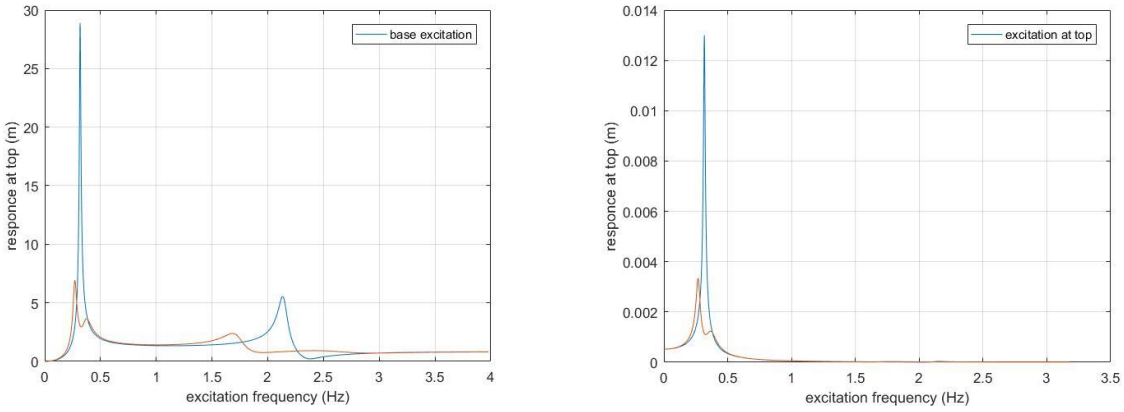

(a) (b)

Figure 4.17: Transfer functions for the displacement at the top of the wind turbine tower, controlled with 2TMDs, due to (a) base excitation, and (b) excitation at top.

In Table 4.2 are the optimum results after the implementation of 2TMDs that control the first 2 natural frequencies of the wind turbine tower before control, with a mass ratio of 10% and a damping ratio of 15%.

Table 4.2: Results after the implementation of 2TMDs of a mass ratio of 10% and a damping ratio of 15%.

Excitation	$\max\left\|u_{top}\right\|\ (m)$	$\max\left\|u_{relativeTMD_1}\right\|\ (m)$	$\max\left\|u_{relativeTMD_2}\right\|\ (m)$
JMA (1995)	0.3264	0.4389	0.1124
TABAS	0.7471	1.2580	0.0894
$\overline{F}_N(t)$	1.3515	1.0183	0.0131

In order to calculate the exact value of the new damping ratio, the isolated system, with the 2 TMDs, is subjected to a free vibration with initial conditions, which in this case are according to the first modal eigenform of the wind turbine tower before control, with the initial conditions of the degrees of freedom of the TMDs to be equal to the respective degrees of freedom of the wind turbine tower which are related. More specifically, the value of the new damping ratio is calculated as in eq. (4.5), where T is the time between two consecutive peaks of the dynamic response of the system, as shown in Figure 4.18 . The new damping ratio of the system equals to 10.86%.

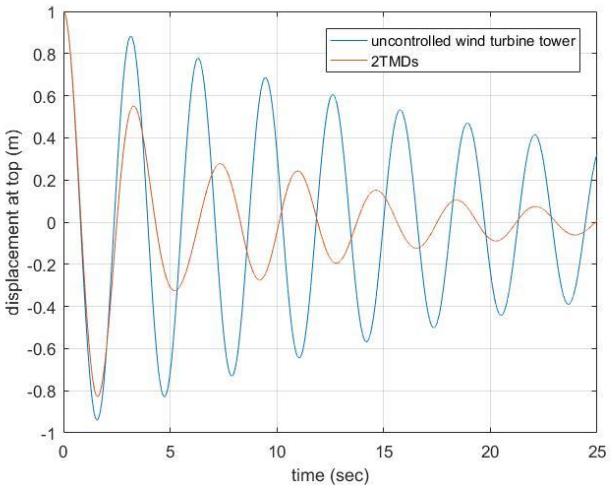

Figure 4.18: Dynamic response of the isolated system, with the 2TMDs, to a free vibration with initial conditions.

4.1.4 Test case 4: Single KDamper placed on top of the wind turbine tower

The mass ratio, the damping ratio and the stiffness k_P have the value 10%, 15% and 454.6 *kN/m* (as in test case 2 with 10% mass ratio) respectively.

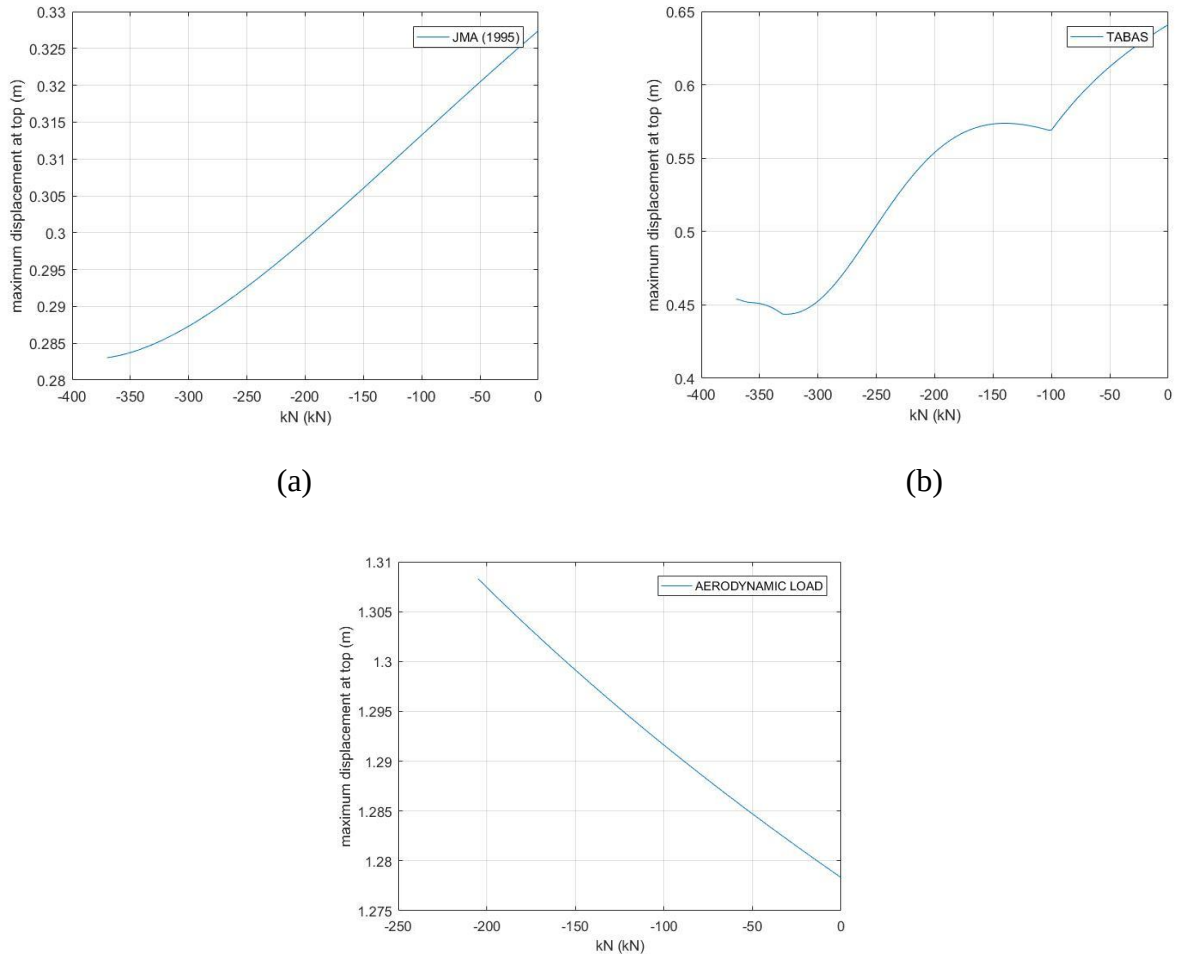

(a) (b)

(c)

Figure 4.19: Variation of the maximum displacement at the top of the wind turbine tower on the negative stiffness element k_N.

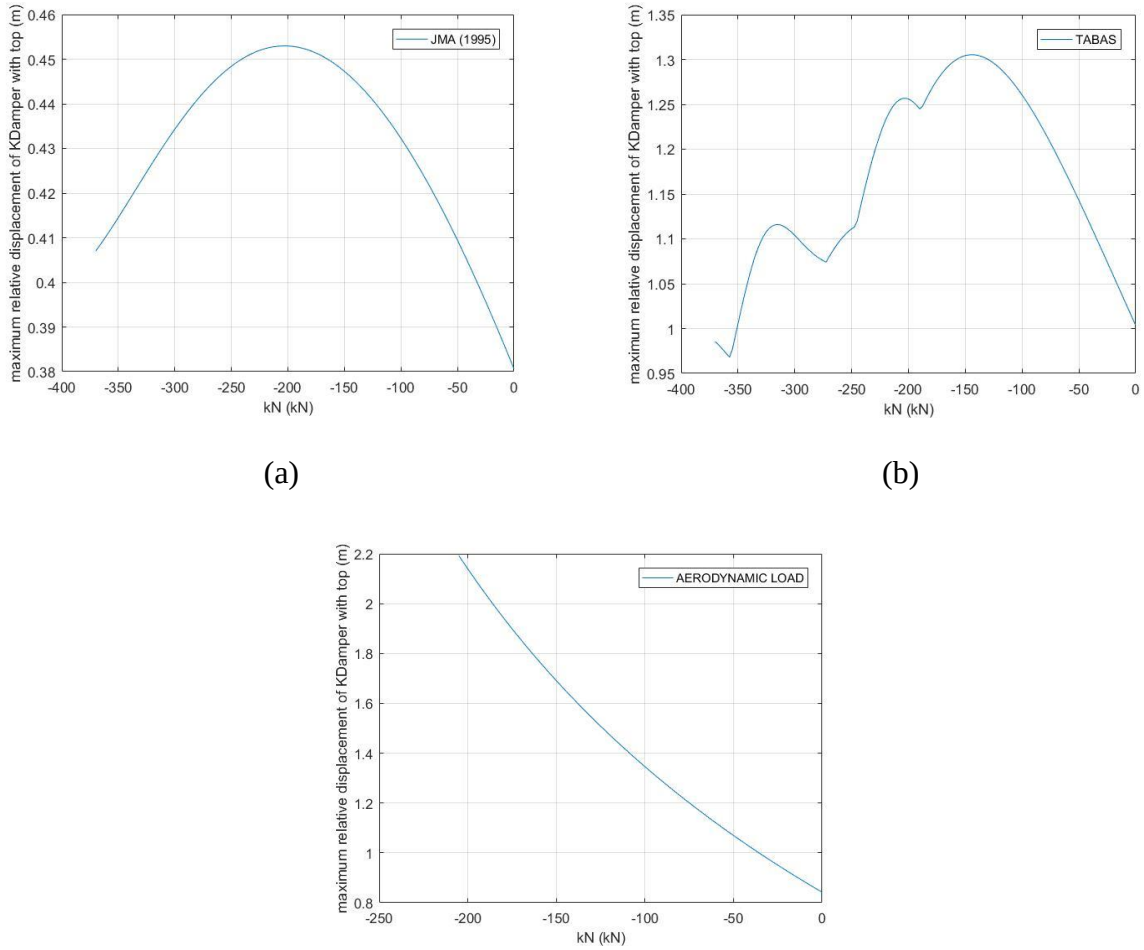

Figure 4.20: Variation of the maximum relative displacement of the KDamper and the top of the wind turbine tower on the negative stiffness element k_N.

In Figure 4.21 the Transfer functions are shown, for the wind turbine tower controlled with a KDamper with a mass ratio of 10%,a damping ratio of 15%, k_P=454.6 *kN/m* and a negative stiffness element of -200 *kN/m*.

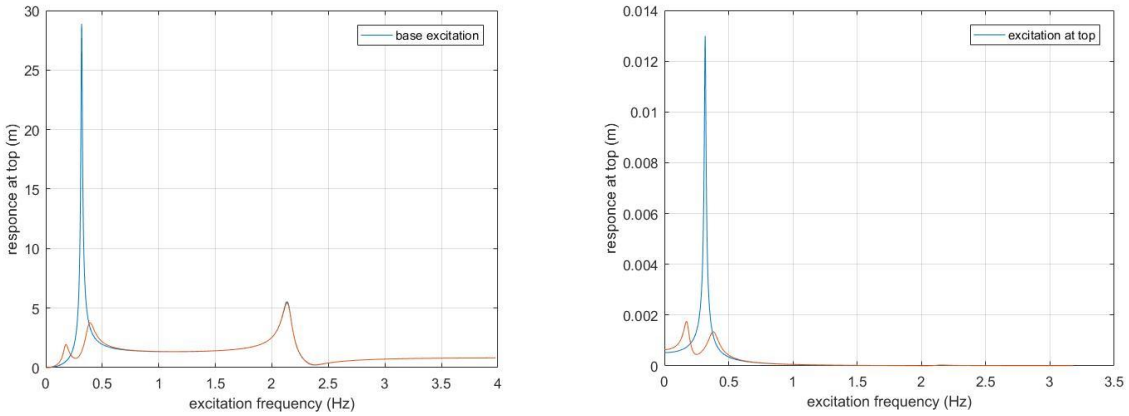

(a) (b)

Figure 4.21: Transfer functions for the displacement at the top of the wind turbine tower, controlled a KDamper, due to (a) base excitation, and (b) excitation at top.

In Table 4.3 the optimum results after the implementation of a KDamper, are presented, with a mass ratio of 10%, a damping ratio of 15%, k_P=454.6 *kN/m* and a negative stiffness element of -200 *kN/m*.

Table 4.3: Results after the implementation of a KDamper of a mass ratio of 10%, a damping ratio of 15%, k_P=454.6 *kN/m* and a negative stiffness element of -200 *kN/m*.

Excitation	$\max\left\|u_{top}\right\|\ (m)$	$\max\left\|u_{relativeKDamper}\right\|\ (m)$
JMA (1995)	0.2991	0.4530
TABAS	0.5539	1.2560
$\overline{F}_N(t)$	1.3074	2.1393

The implementation of the KDamper leads to a new system with reduced displacements along the tower of the wind turbine and higher damping ratio. In order to calculate the exact value of the new damping ratio, the isolated system is subjected to a free vibration with initial conditions, which in this case are according to the first modal eigenform of the wind turbine tower before control with the initial condition of the KDamper equal to the initial condition at the top of the wind turbine tower. However, the new damping ratio of the system cannot be calculated as in the previous Test cases, due to the fact that the maximum values of the response (Figure 4.22), for a free vibration with initial conditions, does not follow an exponential distribution.

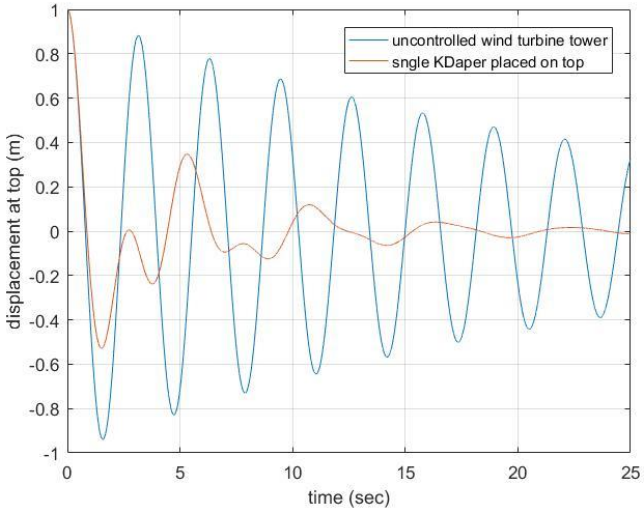

Figure 4.22: Dynamic response of the isolated system, with the KDamper, to a free vibration with initial conditions.

Finally, the static stability margin ε is calculated as in 2.4. With the installed parameters that are presented in 4.1.4, the value for the static stability margin is 1.0283 or 102.83 %.

4.1.5 Test case 5: TMD with an additional mass, that of mtop

In this test case, the additional mass of the TMD is constant and haw the value of 403.22 *tn* which is the additional mass *mtop*, the parameters we have now are the positive stiffness element Kd and the damping ratio of the TMD, ζ.

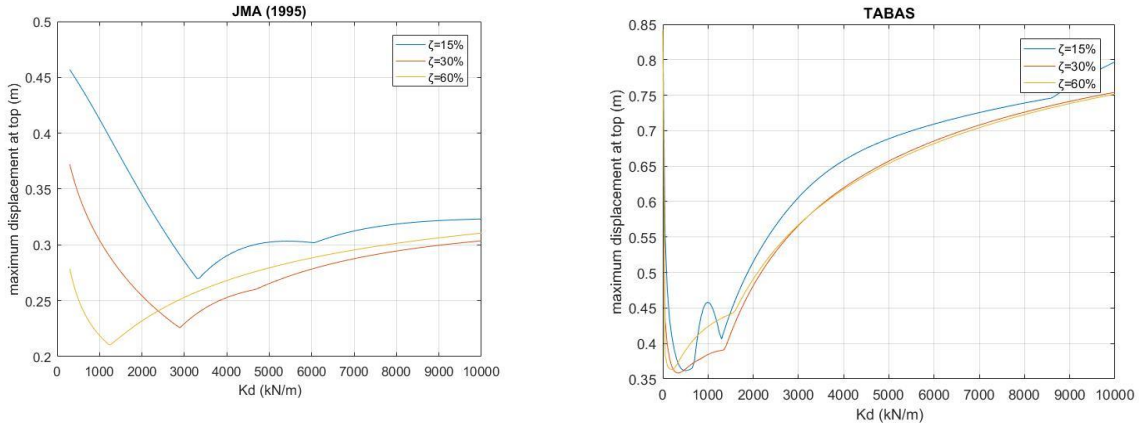

(a) (b)

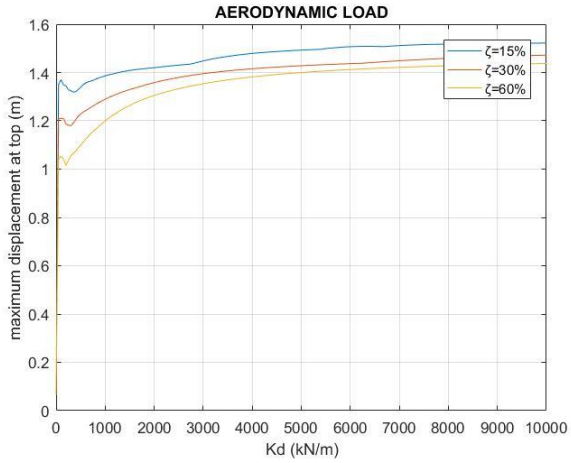

(c)

Figure 4.23: Variation of the maximum displacement at the top of the wind turbine tower on the positive stiffness element *Kd*.

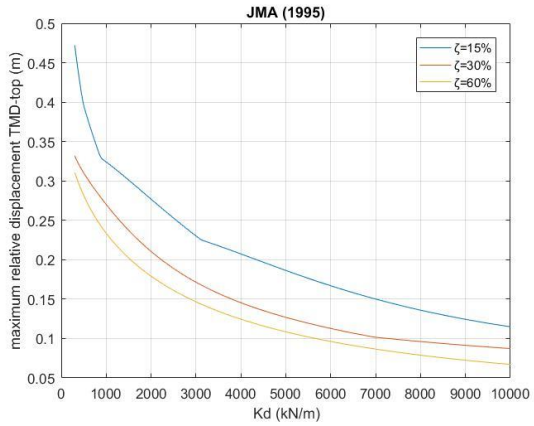

(a)

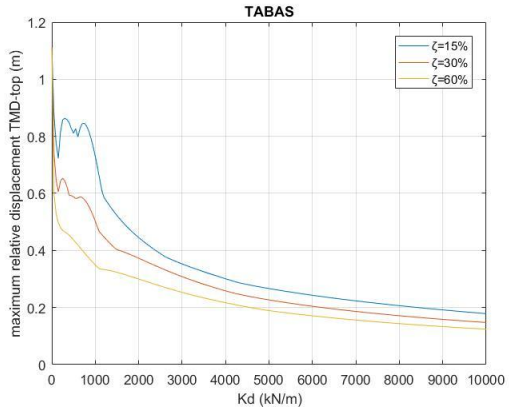

(b)

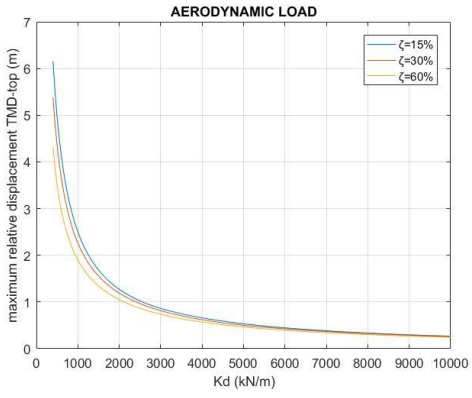

(c)

Figure 4.24: Variation of the maximum relative displacement of the TMD and the top of the wind turbine tower on the positive stiffness element *Kd*.

In Figure 4.26 the Transfer functions are shown, for the wind turbine tower controlled with a TMD the additional mass of 403.22 *tn*, a damping ratio of 30% and a positive stiffness element of 1000 *kN/m*.

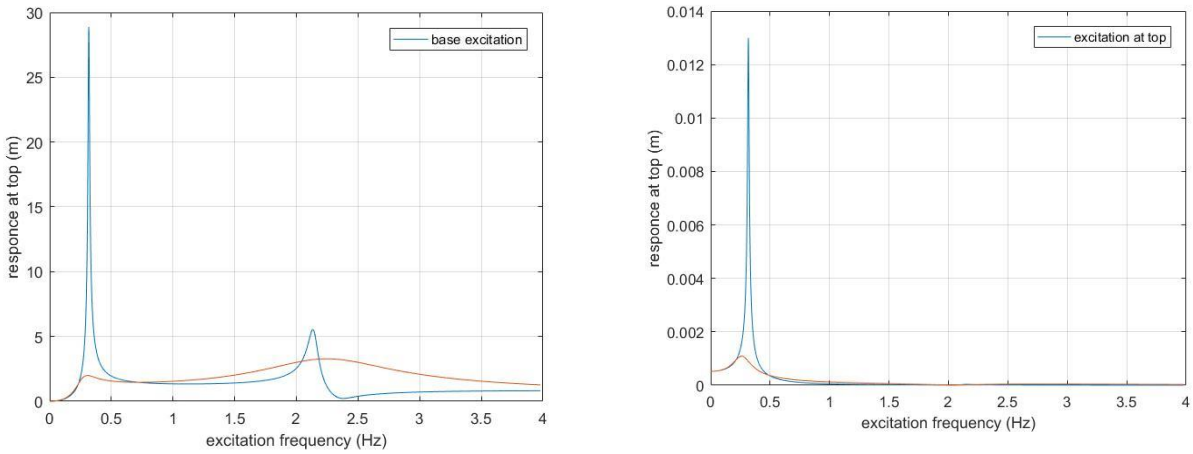

(a) (b)

Figure 4.26: Transfer functions for the displacement at the top of the wind turbine tower, controlled a TMD, due to (a) base excitation, and (b) excitation at top.

In Table the optimum results after the implementation of a TMD, are presented, with an additional mass of 403.22 *tn*, a damping ratio of 30% and a positive stiffness element of 1000 *kN/m*.

Table 4.4: Results after the implementation of a TMD with an additional mass of 403.22 *tn*, a damping ratio of 30% and a positive stiffness element of 1000 *kN/m*.

Excitation	$\max\left\|u_{top}\right\|\ (m)$	$\max\left\|u_{relativeTMD}\right\|\ (m)$
JMA (1995)	0.3041	0.2702
TABAS	0.3845	0.5026
$\overline{F}_N(t)$	1.2893	2.2626

In order to calculate the exact value of the new damping ratio, the isolated system, with the 2 TMDs, is subjected to a free vibration with initial conditions, which in this case are according to the first modal eigenform of the wind turbine tower before control, with the initial conditions of the degrees of freedom of the TMDs to be equal to the respective degrees of freedom of the wind turbine tower which are related. More specifically, the value of the new damping ratio is calculated as in Eq.(48), where T is the time between two consecutive peaks

of the dynamic response of the system, as shown in Figure 22 . The new damping ratio of the system equals to 20.46 %.

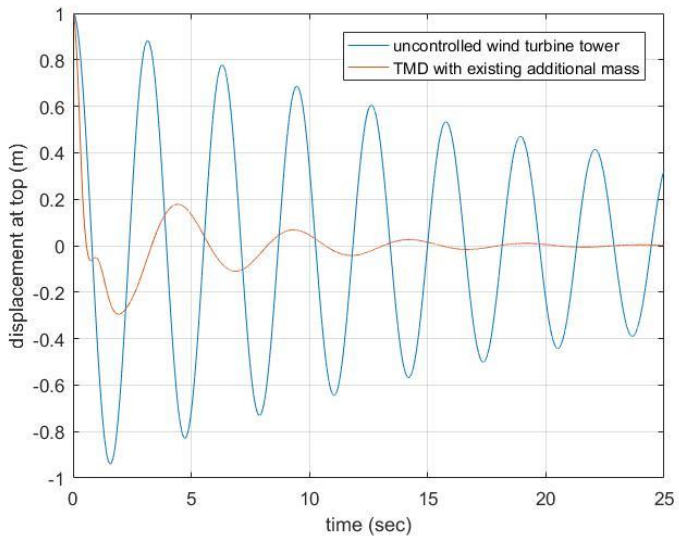

Figure 4.22: Dynamic response of the isolated system, with the KDamper, to a free vibration with initial conditions.

4.2 Comparison of the top displacement

In Table 5, the maximum displacement of the top of the wind turbine tower is presented, for each excitation and test case respectively, as well as the reduction percentage in relation to the top displacement of the uncontrolled wind turbine.

Table 4.4: maximum top displacement for each test case respectively.

Test case	JMA (1995)	TABAS	$\overline{F}_N(t)$
Uncontrolled	0.3682 m	0.9607 m	1.436 m
Single TMD	0.3273 m	0.6408 m	1.2783 m
Reduction	11.10 %	33.29 %	10.98 %
2 TMDs	0.3264 m	0.7471 m	1.3515 m
Reduction	11.35 %	22.23 %	5.88 %
Single KDamper	0.2991 m	0.5539 m	1.3074 m
Reduction	18.77 %	42.34 %	8.95 %
TMD-nacelle	0.3041	0.3845	1.2893
Reduction	17.4 %	59.97 %	10.22 %

5 FINAL REMARKS AND SUGGESTIONS FOR FURTHER RESEARCH

In this present study the dynamic response of a wind turbine tower is examined, with various implementations of TMDs as well as a novel passive vibration isolation system the KDamper. More specifically, the external excitation that were used are 2 seismic excitation, that of JMA (1995) and that of TABAS, and a time-dependent horizontal force $\overline{F}_N(t)$, at the top of the wind turbine tower, due to the wind. The results for each test case in respect of each isolation system have shown:

- The implementation of a TMD at the top of the wind turbine tower tuned with the first natural frequency, before control, with a mass ratio and a damping ratio of 10% and 15% respectively, achieved a reduction at the top displacement 11.10 % for the JMA (1995) seismic excitation, 33.29 % for the TABAS excitation and 10.98 % for the time-dependent horizontal force $\overline{F}_N(t)$, at the top of the wind turbine tower, due to the wind. The new damping ratio of the wind turbine combined with the TMD is 15.68 %.

- The implementation of 2 TMDs placed according to the first 2 modal shapes and more specifically where the first 2 modal shapes presented their maximum values, with a mass ratio and a damping ratio of 10% and 15% respectively, achieved a reduction at the top displacement 11.35 % for the JMA (1995) seismic excitation, 22.23 % for the TABAS excitation and 5.88 % for the time-dependent horizontal force $\overline{F}_N(t)$, at the top of the wind turbine tower, due to the wind. The new damping ratio of the wind turbine combined with the TMD is 10.68 %.

- The implementation of a KDamper at the top of the wind turbine tower with a mas ratio of 10 %, a damping ratio of 15 %, a positive stiffness element of 434.6 kN/m and a negative stiffness element of -200 kN/m, achieved a reduction at the top displacement 18.77 % for the JMA (1995) seismic excitation, 42.34 % for the TABAS excitation and 8.95 % for the time-dependent horizontal force $\overline{F}_N(t)$, at the top of the wind turbine tower, due to the wind. The new damping ratio of the wind turbine combined with the KDamper could not be calculated due to the fact that the peaks of the dynamic response, for a free vibration with initial conditions, does not follow an exponential distribution.

- The implementation of a TMD at the top of the wind turbine tower using as an additional mass that of the mechanical parts (nacelle, rotor and blades) $m_{top} = 403.22\ tn$, with a damping ratio of 30% and a positive stiffness element of 1000 *kN/m*, achieved a reduction at the top displacement 17.40 % for the JMA (1995) seismic excitation, 59.97 % for the TABAS excitation and 10.22 % for the time-dependent horizontal force $\overline{F}_N(t)$, at the top of the wind turbine tower, due to the wind. The new damping ratio of the wind turbine combined with the TMD is 20.46 %.

The KDamper concept can provide a realistic alternative to the existing vibration isolation systems used for the design of wind turbines. The implementation of the KDamper leads to a drastic reduction of the wind turbines dynamic response, in most cases even greater than that of the TMD, offering high damping properties at the same time. The reliability and simplicity of the system are also advantages that render the devise suitable for various technological implementations. Moreover, the inherent non-linear nature of the negative stiffness force can be exploited to offer further potential advantages of the KDamper concept, such as robustness, broadband response and energy sinks.

6 REFERENCES

[1] I. Antoniadis, D. Chronopoulos, V. Spitas, D. Koulocheris, Hyper-damping properties of a stable linear oscillator with a negative stiffness element. *Journal of Sound and Vibration*, **346**, 37-52, 2015.

[2] A. Carella, M. Brennan, T. Waters, Static analysis of a passive vibration isolator with quasi-zero-stiffness characteristic. *Journal Sound and Vibration* **301**, 678-689, 2007.

[3] CEN/TC250 , Eurocode 1: Actions on structures-General actions-Part 1-4: Wind actions. *prEN* 1991-1-4, 2004.

[4] N. Debnath, S. K. Deb, A. Dutta, Multi-modal vibration control of truss bridges with tuned mass dampers under general loading. *Journal of Vibration and Control*, DOI: 10.1177/1077546315571172, 2015.

[5] J.P. Den Hartog, *Mechanical Vibrations, 4th Edition*. McGraw Hill, 1956.

[6] S. Elias, V. Matsagar, T. K. Datta, Effectiveness of distributed tuned mass dampers for multi-mode control of chimney under earthquakes. *Engineering Structures* **124**, 2016.

[7] B. Fitzgerald, B. Basu. Structural control of wind turbines with soil interaction. *Engineering Structures, 111*, 131-151, 2016.

[8] H. Frahm, Device for Damping Vibrations of Bodies. US patent #989958, 1909.

[9] M. O. L. Hansen, Aerodynamics of Wind Turbines. *Earth-scan*, London, 2008.

[10] R. Ibrahim, Recent advances in nonlinear passive vibration isolators. *Journal of Sound and Vibration* **314**, 371–452, 2008.

[11] G. Jackson, Njiri, S. Dirk, State-of-the-art in wind turbine control: Trends and challenges. *Renewable and Sustainable Energy Reviews* **60**, 377-393, 2016.

[12] J. M. Jonkman, Dynamics modeling and loads analysis of an offshore floating wind turbine. *Technical Report* NREL/TP-500-41958, 2007.

[13] M. Lackner , M. Rotea. Passive structural control of offshore wind turbines. *Wind Energy 14(3)*:373-88, 2011.

[14] J. Mayet, H. Ulbrich, First-order optimal linear and nonlinear detuning of centrifugal pendulum vibration absorbers, *Journal of Sound and Vibration* **335**, 34–54, 2015.

[15] W. Molyneaux, Supports for vibration isolation. ARC/CP-322, *Aeronautical Research Council*, Great Britain, 1957.

[16] J. Ormondroyd, J. P. Den Hartog, The Theory of Dynamic Vibration Absorber. *Trans. ASME*, APM-50-7, 9-22, 1928.

[17] D. L. Platus, Negative-stiffness-mechanism vibration isolation systems. *SPIE's International Symposium on Optical Science, Engineering, and Instrumentation*, 98–105, 1999.

[18] A. Quiligan, A. O'Connor, V. Pakrashi, Fragility analysis of steel and concrete wind turbine towers. *Engineering Structures*, **36**, 270-282, 2012.

[19] M. Rahman, Z. C. Ong, W. T. Chong, S. Julai, S. Y. Khoo, Performance enhancement of wind turbine systems with vibration control: A review. *Renewable and Sustainable Energy Reviews* **51**, 43-54, 2015.

[20] E.J. Sapountzakis, P.G. Syrimi, I.A. Pantazis, I.A. Antoniadis, KDamper concept in seismic isolation of bridges. *1st International Conference on Natural Hazards & Infrastructure (ICONHIC 2016)*, Chania, Crete, Greece, June 28-30, 2016.

[21] I. Vassilopoulou, C. Gantes, I. Gkimousis, Response of Cable Networks under Wind Loading. 7*th National Conference on Steel Structures*, Volos, September 29-30 – October 1, 2011.

[22] A. Younespour, H. Ghaffarzadeh, Structural active vibration control using active mass damper by block pulse functions. *Journal of Vibration and Control*, **21**(14), 2787–2795, 2015.